

## The Production and Hydrolysis of Organic Nitrates from OH Radical Oxidation of $\beta$ -Ocimene

Ana C. Morales<sup>1,\*</sup>, Thilina Jayarathne<sup>1,a,\*</sup>, Jonathan H. Slade<sup>2</sup>, Alexander Laskin<sup>1,3</sup>, and Paul B. Shepson<sup>1,3,4</sup>

<sup>1</sup>Department of Chemistry, Purdue University, West Lafayette, IN 47906, USA

5 <sup>2</sup>Department of Chemistry & Biochemistry, University of California San Diego, La Jolla, CA 92093, USA

<sup>3</sup>Department of Earth, Atmospheric, and Planetary Sciences, Purdue University, West Lafayette, IN 47906, USA

<sup>4</sup>School of Marine and Atmospheric Sciences, Stony Brook University, Stony Brook, NY 11794, USA

10 <sup>a</sup>now at: Bristol Myers Squibb, 1 Squibb Drive, New Brunswick, NJ 08901, USA

\*These two authors equally contributed for this work

*Correspondence to:* paul.shepson@stonybrook.edu

**Abstract.** Biogenic volatile organic compounds (BVOCs) emitted by plants represent the largest source  
15 of non-methane hydrocarbon emissions on Earth. Photochemical oxidation of BVOCs represents a  
significant pathway in the production of secondary organic aerosol (SOA), affecting Earth's radiative  
balance. Organic nitrates (RONO<sub>2</sub>), formed from the oxidation of BVOCs in the presence of NO<sub>x</sub>,  
represent important aerosol precursors, and affect the oxidative capacity of the atmosphere, in part by  
sequestering NO<sub>x</sub>. In the aerosol phase, RONO<sub>2</sub> hydrolyze to form nitric acid and numerous water-soluble  
20 products, thus contributing to an increase in aerosol mass. However, only a small number of studies have  
investigated the production of RONO<sub>2</sub> from OH oxidation of terpenes, and among those, few have studied  
their hydrolysis. Here, we report a laboratory study of OH-initiated oxidation of  $\beta$ -ocimene, an acyclic,  
triolefinic monoterpene released during the daytime from vegetation, including forests, agricultural  
landscapes, and grasslands. We conducted studies of the OH oxidation of  $\beta$ -ocimene in the presence of  
25 NO<sub>x</sub> using a 5.5 m<sup>3</sup> all-Teflon photochemical reaction chamber, during which we quantified the total (gas-  
and particle-phase) RONO<sub>2</sub> yield and the SOA yields. We sampled the organic nitrates produced and  
measured their hydrolysis rate constants across a range of atmospherically-relevant pH. The total organic  
nitrate yield was determined to be 383(±97)%, consistent with the available literature regarding the

dependence of organic nitrate production (from RO<sub>2</sub> + NO) on carbon number. We found the hydrolysis  
30 rate constants to be highly pH-dependent, with a hydrolysis lifetime of 51(±13) min. at pH = 4, and 24(±3)  
min. at pH = 2.5, a typical pH for deliquesced aerosols. We also employed high-resolution mass  
spectrometry for preliminary product identification. The results indicate that the ocimene SOA yield  
(<1%) under relevant aerosol mass loadings in the atmosphere is significantly lower than reported yields  
35 from cyclic terpenes, such as α-pinene, likely due to alkoxy radical decomposition and formation of  
smaller, higher-volatility products. This is also consistent with the observed lower particle-phase organic  
nitrate yields of β-ocimene, i.e. 1.5(±0.5)%, under dry conditions. We observed the expected hydroxy  
nitrates by chemical ionization mass spectrometry (CIMS), and some secondary production of the di-  
hydroxy di-nitrates, likely produced by oxidation of the first-generation hydroxy nitrates. Lower RONO<sub>2</sub>  
40 yields were observed under high relative humidity (RH) conditions, indicating the importance of aerosol-  
phase RONO<sub>2</sub> hydrolysis under ambient RH. This study provides insight into the formation and fate of  
organic nitrates, β-ocimene SOA yields, and NO<sub>x</sub> cycling in forested environments from daytime  
monoterpenes not currently included in atmospheric models.

## 1 Introduction

Biogenic volatile organic compounds (BVOCs) constitute the largest flux (88%) of all non-  
45 methane organic compounds to the atmosphere (Goldstein and Galbally, 2007; Guenther et al., 1995,  
2012). Isoprene and monoterpenes account for ~60% of the total global BVOC emissions (Goldstein and  
Galbally, 2007; Guenther et al., 1995). BVOCs participate in chemical reactions with regulated air  
pollutants, including NO<sub>2</sub> and O<sub>3</sub>, and with radical species such as OH and NO<sub>3</sub>, which lead to the  
formation of low volatility oxygenated compounds that partition into aerosol particles and represent  
50 a source of secondary organic aerosol (SOA) (Atkinson and Arey, 2003; Hallquist et al., 2009; Hatakeyama  
et al., 1991; Isaksen et al., 2009; Lee et al., 2016; Monks et al., 2009; Perring et al., 2013; Pye et al., 2015;  
Tuazon and Atkinson, 1990). Globally, the oxidation of BVOCs emitted from forests represents the  
largest source of SOA and affects climate and air quality (Hallquist et al., 2009).

One specific group of BVOC oxidation products of interest is organic nitrates (RONO<sub>2</sub>). By  
55 sequestering NO<sub>x</sub>, RONO<sub>2</sub> slows the production of tropospheric O<sub>3</sub>, but can act as a source of NO<sub>x</sub> and  
O<sub>3</sub> downwind upon further oxidation and decomposition (Browne and Cohen, 2012; Pusede et al., 2015).  
These low volatility, water-soluble compounds are important precursors to and constituents of SOA due  
to their efficient partitioning into the condensed phase (Biesenthal et al., 1997; Fry et al., 2009, 2014;  
Perraud et al., 2012; Rollins et al., 2012). Ambient measurements ~~in forests~~ have indicated that up to 23%  
60 of molecules in organic aerosol contain the RONO<sub>2</sub> functional group, suggesting RONO<sub>2</sub> represent a  
significant fraction of BVOC-derived oxidation products (Ditto et al., 2020; Rollins et al., 2013).  
However, the hydrolysis lifetime of organic nitrates in the aerosol phase (~1-3 hours) is much shorter  
than the lifetime of the aerosol itself to deposition (~1 week), which suggests the contribution of organic  
nitrates to aerosol mass may have been underestimated from the observational data (Romer et al., 2016).

65 It has been shown that these low-volatility oxidation products readily partition from the gas phase  
into the particle phase and undergo further reactions (Perraud et al., 2012). Once in the particle phase,  
organic nitrates can undergo rapid hydrolysis under acid-catalyzed conditions, representing a sink for  
NO<sub>x</sub> in the form of HNO<sub>3</sub> (Bean and Hildebrandt Ruiz, 2016; Darer et al., 2011; Hu et al., 2011; Liu et  
al., 2012; Rindelaub et al., 2015; Takeuchi and Ng, 2019). Hydrolysis rates and the relative contribution  
70 of particle phase hydrolysis as a sink for organic nitrates (compared to reaction with O<sub>3</sub>, OH, photolysis,  
and deposition) vary significantly and depend on molecular structure (Boyd et al., 2015; Zare et al., 2018).  
To date, there are few studies of hydrolysis rate constants for monoterpene-derived organic nitrates  
(Rindelaub et al., 2015). The chemical structure (primary, secondary, and tertiary) can influence the rate  
of hydrolysis lifetimes of organic nitrates (Bean and Hildebrandt Ruiz, 2016; Boyd et al., 2015, 2015,  
75 2017; Darer et al., 2011; Hu et al., 2011; Liu et al., 2012; Ng et al., 2017; Rindelaub et al., 2016b; Takeuchi  
and Ng, 2019; Zare et al., 2018), which is sometimes rapid compared to the lifetime of the particles with  
respect to dry deposition. Thus, more studies are needed to assess the structural dependence of both  
RONO<sub>2</sub> production yields and the hydrolysis rate constants.

Although monoterpenes contribute significantly to the total annual BVOC budget, current models  
80 underestimate the impact of RONO<sub>2</sub> on SOA mass measured in an ambient environment (Pye et al., 2013).  
Importantly, RONO<sub>2</sub> yields for many BVOCs are unknown. Monoterpenes have been shown to produce

more SOA than from isoprene in boreal regions (Lee et al., 2006; Tsigaridis and Kanakidou, 2007). Some of that SOA production from terpenes is now believed to be due to organic peroxides produced from RO<sub>2</sub> + RO<sub>2</sub> reactions involving the 10-carbon RO<sub>2</sub> radicals, when NO concentrations are low (Heinritzi et al., 85 2020). Pratt et al. (2012) showed that, for a temperate mixed-forest in Michigan, isoprene-derived nitrates dominate the daytime simulated gas-phase organic nitrates, however, ~20% is derived from monoterpene nitrates. Of this, nearly one third results from OH-initiated oxidation of β-ocimene, a tri-olefinic monoterpene of high reactivity that is emitted during the daytime (Pratt et al., 2012). To the best of our knowledge, the production of β-ocimene organic nitrates and aqueous-phase processing of its atmospheric 90 oxidation products have not previously been studied.

To expand our understanding of the chemical evolution and fate of monoterpene-derived RONO<sub>2</sub>, we investigated the formation of RONO<sub>2</sub> produced from the OH-initiated oxidation of β-ocimene in the presence of NO<sub>x</sub> using a photochemical reaction chamber. These experiments were conducted as a function of chamber RH to provide insight on aqueous phase partitioning and processing. The aqueous 95 phase processing of these species was explored using linear quadrupole ion trap mass spectrometry to determine hydrolysis kinetics. This study aims to quantify the yields of β-ocimene-derived RONO<sub>2</sub> and the hydrolysis rate constants to better understand how organic nitrates may impact air quality and climate.

## 2 Methods

Experiments were conducted in a custom-made, 5.5 m<sup>3</sup> photochemical reaction chamber 100 consisting of perfluoroalkoxy (PFA)-Teflon walls, PFA-coated endplates, a PFA-coated mixing fan, and UV lamps as described in Chen et al. (1998) and Lockwood et al. (2010). These experiments were conducted as a function of chamber RH, keeping other variables as constant as possible, and at 24(±2) °C. Eighteen experiments were carried out under variable humidity conditions, i.e. <3% up to 70% RH, as listed in Table 1. The maximum humidity achievable in this chamber is 70%, so higher RH is not 105 considered for this study.

Before the experiment, the chamber walls were cleaned by adding ~500 ppb O<sub>3</sub>, irradiating for 1 hour, and flushing with ultra-zero (UZ) air in the dark until the O<sub>3</sub> concentration was ~0 ppb. The O<sub>3</sub> concentration was monitored using a dual beam ozone monitor (2B Technologies, model 205), which is

calibrated using an ozone calibration source (2B technologies, model 306). The chamber RH was  
110 monitored using a LI-COR hygrometer (model 7000). The LI-COR was calibrated from known RH air  
sampled over a saturated  $K_2SO_4$  solution at a fixed temperature. Experiments were started only if the  
chamber particle number concentration was  $<10$  particles per cubic centimeter.

First,  $\beta$ -ocimene ( $\geq 90\%$ , Sigma-Aldrich; (*E*)-/(*Z*)- $\beta$ -ocimene mixture) was introduced to the  
chamber via injection through a T-shaped heated pyrex inlet, through which ultrapure  $N_2$  was used to  
115 transfer the injected  $\beta$ -ocimene via 1/4" PFA tubing at a flowrate of  $5 \text{ L min}^{-1}$ . Formaldehyde (37% v/v  
in water, Sigma) was injected using the same set-up, followed by pure NO (99.5%, Praxair) injected using  
the same set-up without heat. Formaldehyde photolysis serves as an OH precursor in the presence of NO  
(Possanzini et al., 2002). Ammonium Sulfate ( $(NH_4)_2SO_4$ ) seed particles were generated using a 10 wt.%  
 $(NH_4)_2SO_4$  aqueous solution and a commercial atomizer (TSI, Inc., model 3076), and subsequently dried  
120 by passing through a diffusion dryer prior to entering the reaction chamber (as in Rindelaub et al., 2015).  
For humid experiments, chamber RH was adjusted by bubbling UZ air through nano-pure water using a  
commercial bubbler immersed in a temperature-controlled bath. The chamber fan was started during the  
initial injections, ensuring reactants were well mixed. Following mixing, initial concentrations were  
measured before the chamber UV lights were activated. After initial concentrations were measured, the  
125 fan was stopped to minimize wall losses, the chamber lights were activated (time = 0), and real-time  
measurements were obtained. A representative experimental time series is shown in Figure 1, where the  
area between the blue vertical lines represents the time when the UV lights were switched on.

The  $\beta$ -ocimene concentration was quantified using gas chromatography – flame ionization  
detection (GC-FID; HP 5890 Series II) equipped with a gas injection loop. The GC-FID was calibrated  
130 using the same  $\beta$ -ocimene standard injected during the experiments, with gas phase concentrations  
prepared in  $\sim 200$ -liter PFA-Teflon bags. Seven-point calibration curves with  $R^2 > 0.995$  were obtained  
and used for  $\beta$ -ocimene quantitation. NO and  $NO_2$  concentrations were measured using a custom-built  
chemiluminescence  $NO_x$  analyzer (Lockwood et al., 2010). The size-resolved particle mass concentration  
was determined using a scanning mobility particle sizer (SMPS, TSI, Inc., model 3062) directly connected  
135 to the chamber via copper sampling lines. The hydroxy nitrates were quantified using I chemical  
ionization mass spectrometry (CIMS) (Xiong et al., 2015, 2016). The inlet of the CIMS was maintained

at a high relative humidity via saturated UHP N<sub>2</sub> carrier flow to eliminate the effects of water vapor on the CIMS sensitivity (Lee et al., 2016; Xiong et al., 2015). A synthesized  $\alpha$ -pinene hydroxy nitrate standard was used as a surrogate standard to calibrate the CIMS for  $\beta$ -ocimene hydroxy nitrate determination (Rindelaub et al., 2016b; Slade et al., 2017). We note there may be differences in the sensitivity of the instrument towards individual  $\beta$ -ocimene hydroxy nitrate isomers compared to the  $\alpha$ -pinene hydroxy nitrate standard due to differences in polarity and thus binding affinity with I<sup>-</sup> (Iyer et al., 2016; Lopez-Hilfiker et al., 2016). The synthetic  $\alpha$ -pinene hydroxy nitrate standard is a  $\delta$ -hydroxy nitrate (Rindelaub et al., 2016), with expected relatively lower polarity and sensitivity for I<sup>-</sup> adduction compared to its  $\beta$ -analogue, as observed for the  $\beta$ - and  $\delta$ -hydroxy nitrates of isoprene (Iyer et al., 2016). We expect the  $\beta$ -ocimene hydroxy nitrates consist of both sensitive  $\beta$ -hydroxy nitrates and less sensitive configurations, complicating their quantitation. Thus, further study is warranted, e.g., quantum chemical calculations and laboratory experiments (Iyer et al., 2016; Lopez-Hilfiker et al., 2016) to examine how the degree of unsaturation and acyclic nature of the  $\beta$ -ocimene hydroxy nitrate isomers affect their binding affinities with I<sup>-</sup>. O<sub>3</sub> measurements were not possible due to interference in the ozone monitor signal by  $\beta$ -ocimene (Walker and Hawkins, 1952). However, for the NO and NO<sub>2</sub> concentrations present in the chamber, and the J<sub>NO<sub>2</sub></sub> value ( $7 \times 10^{-4} \text{ s}^{-1}$ ), the calculated steady state O<sub>3</sub> concentration was < 1 ppb (considering loss via reaction with NO and  $\beta$ -ocimene) and was not an important reactant in the experiments. Photochemistry was terminated by turning off the chamber lights when one third of the NO concentration remained in the chamber to ensure that  $\beta$ -ocimene oxidation occurred via OH oxidation only, and all RO<sub>2</sub> radicals reacted only with NO (Atkinson et al., 2006; Capouet et al., 2004; Rindelaub et al., 2015).

A series of blank and control experiments was conducted to evaluate i) chamber reactions without  $\beta$ -ocimene or NO, ii) gas- and particle-phase product loss to chamber walls under different RH, and iii) dark reactions of NO<sub>2</sub> with  $\beta$ -ocimene. Chamber reactions without  $\beta$ -ocimene or NO served as blank experiments and confirmed that all the RONO<sub>2</sub> detected during oxidation experiments were produced from the OH-initiated oxidation of  $\beta$ -ocimene in the presence of NO. Additionally, the SOA-particle-phase RONO<sub>2</sub> yields were corrected for wall loss from the a second set of control experiments ( $k_{\text{wall SOA}} = 4.3(\pm 0.3) \times 10^{-5} \text{ s}^{-1}$ ). The gas-phase wall loss rate constant for organic nitrates was determined based on

165 observation of the first-order loss of the CIMS-determined monoterpene hydroxynitrate ( $M = C_{10}H_{17}NO_4$ )  
signal in the dark ( $[M + 1]^+$ ;  $m/z = 342$ ;  $k_{ONg} = 8.8(\pm 2.2) \times 10^{-6} s^{-1}$ ). These experiments were conducted at  
varying relative humidities and the wall loss rate constants ( $k_{wall\ SOA}$ ,  $k_{ONg}$ ) were determined from the  
loss in particle mass concentration and gas-phase concentration over time after the chamber lights were  
turned off. Blank experiments involving sampling from a cleaned chamber reveal no detectable degassing  
170 of organic nitrates from the walls, likely due to hydrolytic loss of adsorbed organic nitrates on the acidic  
walls (e.g. from uptake of  $HNO_3$ ). All experimental datas were corrected for dilution for both the  
photochemistry experiments, and for the post-experiment sampling, based on the sampling time, flow  
rate, and makeup gas flow rate utilized during each experiment ( $k_{avg.\ dilution} = 1.4(\pm 0.1) \times 10^{-5} s^{-1}$  during the  
experiments, and  $4.6(\pm 0.5) \times 10^{-5} s^{-1}$  during sampling  $1.4(\pm 0.1) \times 10^{-3} min^{-1}$ ). To further confirm all  $RONO_2$   
175 was a product of the OH-initiated oxidation in the presence of NO, the third control experiment was  
conducted by injecting  $NO_2$  into the dark chamber (UV lights remained off). The concentration of  $NO_2$   
and ocimene were monitored over time, and the gas- and particle-extracts were analyzed for the presence  
of organic nitrates.

The gas- and particle-phase products were separated and collected for offline analysis by sampling  
180 through a XAD-4 resin-coated 8 channel annular denuder (URG-200) followed by a 47 mm PTFE particle  
filter. The denuder and filter were separately extracted in tetrachloroethylene ( $\geq 99.9\%$ , Sigma-Aldrich)  
immediately following a chamber experiment and stored in a refrigerator at 5 °C. The extracts were then  
analyzed for total organic nitrate concentration using Fourier transform infrared spectroscopy (FTIR,  
Thermo Nicolet 6700) using a 1.00 cm liquid cell, as described by Rindelaub et al. (2015). A quality  
185 control experiment was conducted to determine if degradation of  $RONO_2$  occurred when the samples  
were stored in the refrigerator, and no change in concentration was observed over a 24-hour period.  
Extracts were analyzed by FTIR within 24 hours of extraction and stored in a refrigerator when not in use  
to minimize any degradation or additional reactions *in situ* post-extraction. The organic nitrate  
concentrations were determined using the asymmetric  $-ONO_2$  stretch at  $1640\ cm^{-1}$  (Nielsen et al., 1995),  
190 using an absorption coefficient of  $12900\ L\ mole^{-1}\ cm^{-1}$ . An uncertainty of 7% was applied to the FTIR  
measurements to account for the uncertainty in the absorption coefficient when using a proxy (ethyl hexyl  
nitrate in this study) for  $-ONO_2$  quantitation (Carrington, 1960). After the FTIR analysis, samples were

concentrated to near-complete dryness with ultra-high-purity nitrogen for use in high resolution mass spectrometry analysis for structure elucidation and hydrolysis studies.

195 A series of quality control experiments was performed to evaluate the gas-phase organic nitrate collection efficiency by the denuder, particle transmission efficiency through the denuder, and particle collection efficiency on the filter, as described in Slade et al. (2017). To determine collection efficiency by the denuder, ~200-liter PFA-Teflon bags of known concentrations of ethyl hexyl nitrate were prepared and the concentrations were measured using GC-FID before entering the denuder and immediately after.  
200 The collection efficiency of the denuder was determined to be 100( $\pm$ 9)%. The filter collection efficiency (96( $\pm$ 19)%) was determined by measuring the particle mass concentration before and after the filter. Extraction efficiencies from both the denuder (99( $\pm$ 9)%) and filter (100( $\pm$ 2)%) were determined by measuring the concentration of RONO<sub>2</sub> in 50 mL aliquots of serial extracts, for actual experiments. To account for sample loss during concentration, different aliquots of the gas- and particle-phase extracts  
205 were analyzed at varying points during the solvent evaporation process. As a result, we correct for losses of the organic nitrates due to evaporation during solvent concentration, which contributes a 14% uncertainty to the final concentration. That uncertainty is included in the overall concentration uncertainty discussed below.

To better understand the oxidation products, denuder and filter extracts were analyzed for their  
210 chemical composition via ultra-high-performance liquid chromatography with electrospray ionization time-of-flight tandem mass spectrometry (UPLC-ESI-ToF-MS/MS, Sciex 5600+ TripleToF with Shimadzu 30 series pumps and autosampler) (Slade et al., 2017). The separation was achieved using reverse-phased liquid chromatography (Phenomenex Kinetex EVO C18 column, 100 Å, 100 mm  $\times$  2.1 mm, 5  $\mu$ m) following the gradient elution described in Surratt et al. (2008), and MS analyses were  
215 completed using negative and positive electrospray ionization (ESI) modes with multiple-reaction monitoring (MRM) in the *W* reflectron geometry mode. The mass resolution ( $m/\Delta m$ ) of this mass spectrometer is 25,000 at  $m/z$  195 using an accumulation time of 50 ms. The denuder and filter extracts were reconstituted in a 1:1 v:v solvent mixture of HPLC-grade methanol with 0.1% acetic acid and HPLC-grade water. The gradient elution was performed at 0.3 mL min<sup>-1</sup> with a binary mobile phase system: (A)  
220 0.1% acetic acid in water (B) 0.1% acetic acid in methanol. The 12 min gradient elution was as follows:



the concentration of eluent B was 0% for the first 2 min, linearly increased to 90% from 2 to 10 min, held at 90% from 10 to 10.2 min, and then decreased back to 0% from 10.2 to 12 min (Surratt et al., 2008).

For hydrolysis studies, 3 experiments were selected representing dry, mid, and high RH conditions. The denuder and filter extracts were combined to form a bulk (gas- and particle-phase)  $\beta$ -ocimene nitrate solution and was then concentrated by solvent evaporation. The mixture was then reconstituted in 2.0 mL of an aqueous buffer solution at pH = 2.5, 4.1, and 7.0. To facilitate a direct comparison to results obtained in Rindelaub et al. (2015), the same buffer solutions were used, listed in Table 2. The solution was agitated using a magnetic stir bar and 50  $\mu$ L were extracted every 2 minutes. The extract was then mixed with 50  $\mu$ L of methanol (99.9%, Fisher Chemical). The resulting solution was stirred and immediately analyzed (to avoid any impact of continued hydrolysis) via direct infusion electrospray ionization (ESI) into a Thermo Scientific LTQ XL Linear Ion Trap mass spectrometer operated in negative ionization mode. The hydrolysis rate constants were determined from the first-order decay of various organic nitrate-related functional groups monitored by MS<sup>2</sup> fragmentation experiments. Briefly, fragmentation of the isolated molecular ion  $m/z$  214.1 (C<sub>10</sub>H<sub>16</sub>NO<sub>4</sub>, expected first-generation oxidation product) was monitored at the instrument setting of collisional dissociation energy (CE) of 35 eV. The  $m/z$  46 (NO<sub>2</sub><sup>-</sup>) and 62 (NO<sub>3</sub><sup>-</sup>) mass fragments were used to quantify relative concentrations of C<sub>10</sub>H<sub>16</sub>NO<sub>4</sub> species as a function of the hydrolysis time. The exponential decrease in peak area of  $m/z$  46 (NO<sub>2</sub><sup>-</sup>) was used to quantify the observed hydrolysis rate constant, which is effectively the weighted average for the different structural isomers present in the solution, weighted by their relative concentrations. The  $m/z$  62 (NO<sub>3</sub><sup>-</sup>) fragment was used as a confirmation ion.

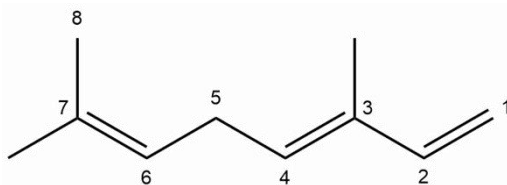
### 3 Results and Discussion

#### 3.1 Organic nitrate yields

A primary objective for this study is quantitative measurements of organic nitrate yields from OH reaction with  $\beta$ -ocimene, where the yields are defined as the concentration of RONO<sub>2</sub> produced ( $\Delta$ RONO<sub>2</sub> in ppb) relative to the concentration of BVOC consumed ( $\Delta$ BVOC in ppb), i.e.,  $Y_{\text{RONO}_2} = \Delta\text{RONO}_2/\Delta\text{BVOC}$  (Slade et al., 2017), corrected for losses of the organic nitrates. In our experiments, all peroxy radicals react with NO. Thus



250  $-\text{d}[\beta\text{-ocimene}]/\text{dt} = k_2[\text{RO}_2][\text{NO}]$ , where  $k_2 = k_{2a} + k_{2b}$ , and  $\text{d}[\text{RONO}_2]/\text{dt} = k_{2b}[\text{RO}_2][\text{NO}]$ . Thus,  $(\text{d}[\text{RONO}_2]/\text{dt})/(-\text{d}[\beta\text{-ocimene}]/\text{dt}) = k_{2b}/k_2$ . A plot of  $\Delta[\text{RONO}_2]$  vs  $-\Delta[\beta\text{-ocimene}]$  yields the  $\text{RO}_2$ -weighted average “branching ratio”,  $k_{2b}/k_2$ , for the  $\text{RO}_2$  radicals produced when OH reacts with  $\beta$ -ocimene in the presence of  $\text{O}_2$ . We utilized the method of Kwok and Atkinson, (1995) to estimate the fraction of time that OH adds to any of carbon #1, 2, 3, 4, 6, or 7, with numbers as shown here.



(*E*)-3,7-dimethylocta-1,3,6-triene

255

Because of the multiple double bonds at which OH can add, and because of the resonance structures of the multiple allylic radicals produced when OH adds to C#s 1 or 4 (as shown for the most prevalent addition point, C4, in Figure 2), there are 10 possible main organic nitrate isomers, for each stereoisomer, i.e. the *cis*- or *trans*- $\beta$ -ocimene, complicating the product analysis. Additional isomers may form from H-  
 260 abstraction from the C-5 methylene group, but these are of less significance than the isomers produced from OH-addition to the double bond. The measured total hydroxynitrate, gas-, and particle-phase total organic nitrate yields under different RH are shown in Figure 3. Yields are corrected for dilution in the chamber, loss to the chamber walls, loss during preconcentration, and hydroxynitrate consumption by reaction with OH (Rindelaub et al., 2015; Slade et al., 2017). The error bars on individual points reflect  
 265 the propagated analytical uncertainties of the yields, incorporating all known uncertainties. The analytical uncertainty accounts for analytical errors associated with all the steps involved in sample collection, extraction, and analysis, including denuder and filter extraction and collection efficiencies, uncertainty in the FTIR calibration when using a proxy for  $-\text{ONO}_2$  quantitation, dilution, wall loss, and consumption by OH. In Figure 3, we see that the observed total  $\text{RONO}_2$  yield, and that for both gas- and aerosol-phases,  
 270 and for the CIMS-determined hydroxy nitrates, are RH dependent, decreasing by  $\sim 2$  over the range studied ( $\sim 3$ -70% RH). The decrease indicates that hydroxy nitrates partition to the aerosol phase, where

they are lost by hydrolysis, which was previously observed in the case of  $\alpha$ -pinene (Rindelaub et al., 2015). At higher RH, there will be more water associated with the particles, and the hydroxy nitrates are then more particle-soluble (Rindelaub et al., 2015). If we then extrapolate to 0% RH, the extent of particle-  
275 phase loss will be minimized, and thus the intercept represents the determined lower limit to the yield, assumed to represent the fraction of peroxy radicals reacting with NO that react to produce RONO<sub>2</sub>. The intercept for the total RONO<sub>2</sub> yield, as shown in Figure 3, is ~~33~~38(~~±9~~±7)%, represented by the y-intercept of the black symbols in Figure 3a. In Figure 4, we present a summary of a range of previous observations of branching ratios for alkanes, alkenes, isoprene and the two terpenes for which we have determined the  
280 total yield (assumed RO<sub>2</sub>-weighted average branching ratio). It is shown that the branching ratio for  $\beta$ -ocimene- and  $\alpha$ -pinene-derived RONO<sub>2</sub> follows the trend observed for simple alkanes, within the uncertainty of the measurements (Arey et al., 2001; Rindelaub et al., 2015; Teng et al., 2015, 2017; Xiong et al., 2015).

We found that the first-generation hydroxy nitrates exist primarily in the gas phase (red markers  
285 in Figure 3a), which is consistent with the low SOA yield, shown in Figure 5. Although the total RONO<sub>2</sub> yield of  $\beta$ -ocimene is greater than that for  $\alpha$ -pinene oxidation, the particle phase organic nitrate yield is much larger in the  $\alpha$ -pinene case (Rindelaub et al., 2015). This is likely due to the fact that the SOA yield is much larger for  $\alpha$ -pinene (34±12%; Rindelaub et al., 2016a), since, as discussed in the next section,  $\beta$ -ocimene oxidation produces smaller, more volatile, acyclic oxidation products. However, some of the low  
290 particle phase RONO<sub>2</sub> yield must occur because of the hydrolysis in the aerosol phase. The relatively low SOA yield for  $\beta$ -ocimene can be attributed to the alkoxy radical decomposition products that produce the remaining ~~67~~62% of the first-generation oxidation products following the OH-initiated pathway in the presence of NO<sub>x</sub>, e.g. as shown producing methyl vinyl ketone and 2-methyl-2-pentenal, in Figure 2. These decomposition products are expected to be primarily C6- and smaller carbonyl compounds, of  
295 much greater volatility than the  $\beta$ -ocimene hydroxy nitrate. This occurs in the case of this linear tri-alkene, because scission of the C-C bond at the  $\alpha$ -position to the alkoxy radical breaks the carbon chain into smaller chain carbonyl compound products, as shown in Figure 2. As previously stated, the expected first-generation oxidation products (Figure 2) are in the upper range of semi-volatile species, confirming their preferential presence in the gas phase (Donahue et al., 2011).

300 The CIMS-measured hydroxynitrate yields (green markers in Figure 3a) are lower than the total gas-phase RONO<sub>2</sub> yield (from FTIR), likely due to a lower CIMS sensitivity to the β-ocimene hydroxy nitrates than assumed, using the α-pinene hydroxy nitrate standard used as a proxy. However, it is important to note that we expect all organic nitrates in this system to be hydroxy nitrates. In this regard, it is important that the CIMS-observed hydroxy nitrate concentration decayed to the same relative extent  
305 as for the FTIR-determined total, as shown in Figure 3. When the hydroxynitrate undergoes hydrolysis, the reaction proceeds likely via SN1 unimolecular nucleophilic substitution, as discussed in (Rindelaub et al., (2015)). The nitrooxy functional group serves as a leaving group and is replaced with a hydroxyl group, ultimately forming a diol. We calculated the vapor pressure of the diol produced from hydrolysis of Compound A in Figure 2, using SIMPOL (Pankow and Asher, 2008), and obtained  $5.5 \times 10^{-8}$  atm at  
310 20°C, which is identical to that calculated for Compound A itself. However, it is likely that the Henry's Law constant for dissolution of the diol into water will be greater than that of Compound A (Shepson et al., 1996), effectively increasing the partitioning into the aerosol phase.

### 3.2 SOA yields

Aerosol-mass-dependent secondary organic aerosol yields ( $Y_{\text{SOA}}$ ) were calculated using the  
315 change in aerosol mass concentration ( $\Delta M$  in  $\mu\text{g m}^{-3}$ ) relative to the β-ocimene mass consumed ( $\Delta\text{BVOC}$  in  $\mu\text{g m}^{-3}$ ), i.e.,  $Y_{\text{SOA}} = \Delta M / \Delta\text{BVOC}$  (Slade et al., 2017). The aerosol mass concentration was derived from the SMPS data, assuming spherical particles of  $1.25 \text{ g cm}^{-3}$  density (based on Ng et al., 2006), as shown in Figure 1. The measured SOA yields as a function of aerosol mass concentration and chamber RH are shown in Figure 5a, where the error bars reflect the propagated analytical uncertainty of the yields  
320 when considering the wall loss and dilution correction. While there is an apparent increase in aerosol yield with increasing humidity, it is not statistically significant (Figure 5a). We calculate from the data in Figure 5a that the SOA yield from OH oxidation of β-ocimene is less than 1% for typical aerosol mass concentrations in a moderately polluted forested environment,  $\sim \leq 10 \mu\text{g m}^{-3}$  (Hallquist et al., 2009). These yields are much lower than reported SOA yields from α-pinene ( $34 \pm 12\%$ ), (Rindelaub et al., 2015). Again,  
325 we hypothesize that this is related to structural differences of the alkoxy radicals, as shown in Figures 2 and 6, specifically that in the β-ocimene case, cleavage of the α-C-C bond leads to two smaller radical

fragments (Figure 2) and ultimately more volatile smaller carbonyl compounds (Gaona-Colmán et al., 2018; Reissell, 2002). For  $\alpha$ -pinene, most of the products retain a C10 backbone (Rindelaub et al., 2016a) due to ring opening reaction resulting from the  $\alpha$ -carbon-carbon bond cleavage. To better understand the SOA yields, two-product absorptive partitioning model fits of the data from this study were compared to model fits and SOA yields of similar acyclic, tri-olefinic monoterpenes, shown in Figure 5b (Böge et al., 2013; Griffin et al., 1999; Hoffmann et al., 1997). The 2-product model fit parameters are as follows:  $\alpha_1 = 0.1768$ ,  $\alpha_2 = 0.0139$ ,  $k_1 = 0.0020$ ,  $k_2 = 0.1698$ . On average, the SOA yields in this study at all relative humidity values are less than that measured from  $\beta$ -ocimene photooxidation in a previous study, likely due to the absence of O<sub>3</sub> in our study (Hoffmann et al., 1997). Additionally, three experiments were conducted without seed aerosol to investigate the role of the inorganic seed aerosol. It was found that there is no apparent dependence of the yields in the seeded experiments versus the non-seeded experiments. We find that the SOA yields for myrcene (also a linear triene) were greater than those for  $\beta$ -ocimene (Böge et al., 2013). This is likely because of the two terminal double bonds on myrcene that would result in a greater fraction of C<sub>9</sub> carbonyl compound products.

Low-volatility/water soluble organic nitrates can partition to the particle phase and contribute to the SOA mass. The estimated vapor pressure ( $V_P$ ) of the  $\beta$ -ocimene hydroxy nitrate is  $5.6 \times 10^{-8}$  atm at 20°C (Pankow and Asher, 2008), which is in the upper range of semi-volatile species, explaining the low aerosol phase organic nitrate yields. Furthermore, the average saturation mass concentration ( $C^*$ ) of  $\beta$ -ocimene hydroxy nitrates determined from the low RH (<3%) experiments in this study was found to be 4000  $\mu\text{g m}^{-3}$ , which is in agreement for species that exist almost entirely in the gas-phase (Seinfeld and Pandis, 2016). This is in contrast to our experiments with  $\alpha$ -pinene derived hydroxy nitrates, for which most were in the aerosol phase, at low relative humidities. (Rindelaub et al., 2015). The estimated  $V_P$  of the  $\alpha$ -pinene hydroxy nitrate shown in Figure 6 is  $8.6 \times 10^{-8}$  atm at 20°C (Pankow and Asher, 2008), which is greater than that of the  $\beta$ -ocimene hydroxy nitrate because of the ring in the C10 structure. However, the oxidation of  $\alpha$ -pinene results in ring opening rather than fragmentation (as shown in Figure 6), in the case of ocimene. Thus, the first-generation oxidation products from  $\alpha$ -pinene will tend to be C10 species of lower vapor pressure than for the lower carbon number products in the ocimene case. The lower vapor pressure higher carbon-number products likely lead to the greater aerosol yield ( $\sim \times 6$ ) for  $\alpha$ -pinene, which

355 in turn increased the partitioning of organic nitrates to the aerosol phase (Rindelaub et al., 2015). It is now well known that aerosol liquid water can also influence the SOA growth. In the ambient environment, as relative humidity increases (and as aerosol ages), the aerosol liquid water also increases (Carlton and Turpin, 2013), driving uptake of water-soluble oxidized organic compounds (WSOC). However, in the photochemical smog chamber used in this study, the extent of VOC oxidation is very low (i.e. with mostly  
360 primary products, by design), and the resulting aerosols likely have relatively low O:C, resulting in a small correlation between relative humidity and aerosol yield, as shown in Figure 5.

The gas- and particle-phase extracts were analyzed using UHPLC-ToF-MS/MS to elucidate oxidation product structures. In Figure 7, the selected ion chromatograms (SIC) of expected oxidation products from ESI negative mode are presented for both the filter (7a) and denuder (7b) extracts for  
365 experiment #6. Tentative structures of the selected ions are shown, but the structures of these molecules were not confirmed with authentic standards. The arrangement of functional groups may vary depending on the position of the addition of the hydroxyl group to the original  $\beta$ -ocimene reactant. As shown in the light blue trace in Figure 7, we do observe the dihydroxy dinitrate, although the effective gas phase concentration could not be determined. As described above, we do correct for loss of the primary hydroxy  
370 nitrate by reaction with OH. In the case of the dinitrate, production would increase the effective measured organic nitrate yield. On the other hand, we also observe some of the trihydroxy nitrate, as shown in Figure 7, indicating partial hydrolysis of the dinitrate. In this case, the product is neutral in its impact on the measured organic nitrate yield, and as discussed below, given the hydrolysis rate constants, and the time scale of the experiments, it is likely that there is some hydrolysis of the primary organic nitrates to  
375 the corresponding diol, leading to the negative slope observed in Figure 3. We hypothesize that the smaller (C6 or C4) fragments produced during the oxidation (not seen in our analysis) were lost during the solvent evaporation process, due to their high volatility.

### 3.3 Aqueous phase hydrolysis

The observed decrease of the RONO<sub>2</sub> yields with increasing RH (Figure 3) indicates acid-  
380 catalyzed hydrolysis in the aerosol phase. To date, there have only been hydrolysis rate constant determinations for a few organic nitrates (Baker and Easty, 1950; Bean and Hildebrandt Ruiz, 2016; Boyd

et al., 2015; Darer et al., 2011; Fisher et al., 2016; Hu et al., 2011; Liu et al., 2012; Pye et al., 2015; Zare et al., 2018), including the  $\alpha$ -pinene hydroxynitrate (Rindelaub et al., 2015) and a range of isoprene-derived hydroxynitrates (Jacobs et al., 2014). Here we studied the aqueous phase hydrolysis kinetics (in  
385 bulk aqueous solution, adjusted for pH) of ocimene nitrates by examining the decay of the gas- and particle-phase organic nitrate products using mass spectrometry. In Table 3, we tabulated the hydrolysis rate constants reported in the literature, for a wide range of organic nitrates, along with those determined here, indicating the solution pH, where known. There are a number of observations that can be made, most clearly, that tertiary nitrates generally have very short hydrolysis lifetimes, that a  $\beta$ -hydroxy group  
390 shortens the hydrolysis lifetime, and that the hydrolysis lifetimes decrease with decreasing pH. We conducted measurements of the aqueous hydrolysis rate constants for the sum of the  $\beta$ -ocimene nitrates from the combined denuder and filter extracts for all experiments with RH < 3%, via electrospray MS/MS, as a function of the solution pH. In Figure 8, we plot  $\ln A_0/A_t$  vs  $t$ , in seconds, where zero is an arbitrary starting point for the pH-adjusted (buffered) samples. The resulting plots were linear, as expected for a  
395 first order exponential decay. The slope of each line is equal to the first-order hydrolysis rate constant. The symbols in this figure represent replicates for each pH, and each panel is a different pH, all on the same scale for each pH. As shown in Figure 8, the rate constants increase significantly, i.e. by  $\sim \times 12$ , over the range pH = 7.0 to pH = 2.5. These bulk rate constants represent those for the yield-average weighted organic nitrates produced. As there are many structural isomers produced during the OH-initiated  
400 oxidation of  $\beta$ -ocimene (Figure 2), additional work is necessary exploring the structural dependence on hydrolysis rates. The initial concentration in the bulk solution is likely dominated by tertiary hydroxy nitrates, but the concentration and ionic strength for our experiments would be very low compared to those present within individual particles. This may impact the results, as discussed by Liu et al. (2020). The hydrolysis rates for primary and secondary hydroxy nitrates are likely slower than those of tertiary  
405 hydroxy nitrates, but increased ionic strength in the particle phase could contribute to more rapid hydrolysis and shorter lifetimes (Bean and Hildebrandt Ruiz, 2016; Boyd et al., 2015; Darer et al., 2011; Fisher et al., 2016; Hu et al., 2011; Jacobs et al., 2014; Liu et al., 2012, 2020; Pye et al., 2015; Takeuchi and Ng, 2019; Zare et al., 2018). Additional work investigating the hydrolysis rates of individual isomers (primary, secondary, tertiary) would be useful to understand the structural dependence of hydrolysis rates.

410 It is however interesting and useful that the linear chain nitrates studied here have very similar hydrolysis rates constants compared to those for the cyclic structure (with a distant -OH) of the  $\alpha$ -pinene hydroxy nitrate studied by Rindelaub et al. (2015).

In Figure 9, we plot our data for the  $\beta$ -ocimene nitrates, along with those for the  $\alpha$ -pinene nitrate studied by Rindelaub et al. (2015), as a function of pH. The equation for the best-fit line in Figure 9 is  
415  $\log_{10} k = -(0.24(\text{pH}) + 2.58)$ , for  $\beta$ -ocimene. This shows that the natural lifetime against hydrolysis is 51 minutes at  $\text{pH} = 4$  and decreases to 11 minutes at  $\text{pH} = 1$ . These are very short, compared to the lifetime of fine mode aerosol, i.e.  $\sim 1$  week. Thus, we might expect that the ambient aerosol phase concentration of such hydroxy nitrates might typically be quite low, even though their uptake from the gas phase may have contributed significantly to aerosol mass, because they have subsequently transformed to diols. We  
420 also see that the hydrolysis lifetimes are very similar for the quite structurally different cyclic  $\alpha$ -pinene nitrate and acyclic  $\beta$ -ocimene nitrates, shown in Table 3. This implies that these values may be close to representative for a range of hydroxy nitrates. This rapid aqueous-phase hydrolysis points to the possible underestimation of aerosol phase organic nitrates under ambient conditions (Ditto et al., 2020). As hydroxy nitrate production can represent an important fate for daytime oxidation of isoprene and terpenes  
425 in forested environments, the uptake of these compounds into acidic aerosol followed by hydrolysis can represent an important mechanism for conversion of  $\text{NO}_x$  to  $\text{HNO}_3$ , as discussed in Romer Present et al. (2019) and Zare et al. (2018).

While the fate of the resulting diol in solution is unclear, there is a range of possible processes in the aqueous phase, including OH attack and oligomerization. Further oxidation of these olefinic diols  
430 would likely result in fragmentation, which might then cause product release into the gas phase (Otto et al., 2017). Diols, and these olefinic diols, can also undergo oligomerization to form even lower volatility products which may have profound effects on the overall aerosol properties, such as viscosity and rate of diffusion (Glasius and Goldstein, 2016; Slade et al., 2019). The presence of oligomers from diols has previously been identified, but molecular characterization is quite limited (Stropoli et al., 2019). Careful  
435 investigation of the structures of these oligomers is necessary to develop reliable predictive models of SOA formation (Budisulistiorini et al., 2017; Pye et al., 2013; Surratt et al., 2007).



## 4 Atmospheric Implications and Conclusions

The production of organic nitrates serves as an important sink for gas phase  $\text{NO}_x$ . The first generation organic nitrate products are relatively high vapor pressure and, for the polyunsaturated terpene  $\beta$ -ocimene, are subject to further gas phase oxidative loss, to produce smaller, but more oxidized products (Bateman et al., 2011). While the main products of that oxidation will be hydroxy nitrooxy carbonyl compounds of lower carbon number, and thus perhaps higher vapor pressure, the yield of dihydroxy dinitrates will be significant. The latter compounds will be much lower vapor pressure, e.g. that for Compound B shown in Figure 2, is  $2.4 \times 10^{-12}$  atm at 20 °C (Pankow and Asher, 2008), low enough that it should rapidly undergo uptake into the aerosol phase, followed by hydrolysis to produce a 10-carbon tetrol and  $\text{NO}_3^-$ . However, the extent to which the gas phase oxidation of the first generation olefinic hydroxy nitrates re-releases  $\text{NO}_x$  needs to be studied from laboratory experiments with the pure compounds. The organic nitrates will undergo hydrolysis in the particle phase, transforming from a hydroxynitrate to a diol. The nitrooxy group will be released as the nitrate ion, which can impact regional nitrogen cycling by either remaining in the particle phase (at certain pHs) or be released as gas phase nitric acid (at very high particle acidities). In either case,  $\text{NO}_x$  has been permanently removed from the system (Galbavy et al., 2007; Rindelaub et al., 2015; Romer Present et al., 2019; Suarez-Bertoa et al., 2012; Zafiriou and True, 1979). Therefore, knowledge of the hydrolysis rate constants, especially for isoprene nitrates, is badly needed. The relatively large organic nitrate yield ( $338 \pm 97\%$ ) in combination with the rapid aqueous-phase hydrolysis both tend to make organic nitrate production an important sink for  $\text{NO}_x$  in terpene-impacted forest environments. In addition, the light dependent emission rate of  $\beta$ -ocimene suggests that in dense forest environments, like that of the University of Michigan Biological Station (Pratt et al., 2012), there could be steep vertical gradients in organic nitrate concentrations between canopy and ground, exceeding that of the other terpene nitrates modelled in Schulze et al. (2017). It is thus necessary to further asses the organic nitrate yield values, hydrolysis rate constants, and major oxidation products for a range of terpenes to fully understand the impact of their oxidation on the fate and distribution of  $\text{NO}_x$ .

These results suggest that  $\beta$ -ocimene hydroxy organic nitrates may be an important sink for gas phase  $\text{NO}_x$  in forest environments. Further work should be done to examine the structural dependence of

465 hydroxy nitrate hydrolysis kinetics, e.g. the difference between  $\beta$ -hydroxy and  $\delta$ -hydroxy nitrates. Previous work has determined thermodynamic stabilities of structurally different organic nitrates (primary, secondary, tertiary) based on acid-catalyzed hydrolysis, where tertiary organic nitrates are less stable than primary or secondary organic nitrates at atmospherically-relevant pHs, suggesting potential differences in hydrolysis rates between  $\beta$ -hydroxy and  $\delta$ -hydroxy nitrates (Hu et al., 2011). Differences  
470 between the hydrolysis rates of  $\beta$ -ocimene organic nitrates from  $\text{NO}_3$  and OH-initiated oxidation should be explored, as significant differences in the hydrolysable fractions have been shown between organic nitrates formed from  $\text{NO}_3$  and OH-initiated oxidation of both  $\alpha$ - and  $\beta$ -pinene (Takeuchi and Ng, 2019), and daytime  $\text{NO}_3$  concentrations can be relevant in forests like that of University of Michigan Biological Station (Pratt et al., 2012; Schulze et al., 2017). It is necessary to understand the SOA components  
475 produced during this oxidation to better predict aqueous phase processing. Further work on the condensed phase chemistry of alcohols and olefinic oxygenated compounds in the aerosol phase is necessary.

## 6 Acknowledgement

We would like to thank Dr. Chloé de Perre and Prof. Linda Lee of the Department of Agronomy at Purdue University for the use of UHPLC-MS instrumentation and analysis assistance. We also would  
480 like to thank Tad Kleindienst and John Offenberg of the EPA for assistance with the denuder-based filter set-up. Dr. Anusha Hettiyadura and Krissy Morgan are thanked for assistance with hydrolysis studies and chamber experiments. We acknowledge Dr. Hartmut Hedderich of the Jonathan Amy Facility for Chemical Instrumentation (JAFCI, Purdue University) for access to FTIR instrumentation and T. Miller (Birck Nanotechnology Center, Purdue University) for nano-pure water. This material is based upon work  
485 supported by the National Science Foundation Graduate Research Fellowship Program under Grant No. (DGE-1333468) and an NSF Grant No. (1550398-CHE) in support of the Shepson group. Any opinions, findings, and conclusions or recommendations expressed in this material are those of the author(s) and do not necessarily reflect the views of the National Science Foundation.

## References

- 490 Arey, J., Aschmann, S. M., Kwok, E. S. C. and Atkinson, R.: Alkyl Nitrate, Hydroxyalkyl Nitrate, and Hydroxycarbonyl Formation from the  $\text{NO}_x$  -Air Photooxidations of  $\text{C}_5$  - $\text{C}_8$  *n* -Alkanes, *J. Phys. Chem. A*, 105(6), 1020–1027, doi:10.1021/jp003292z, 2001.
- Atkinson, R. and Arey, J.: Gas-phase tropospheric chemistry of biogenic volatile organic compounds: a review, *Atmos. Environ.*, 37, 197–219, doi:10.1016/S1352-2310(03)00391-1, 2003.
- 495 Atkinson, R., Baulch, D. L., Cox, R. A., Crowley, J. N., Hampson, R. F., Hynes, R. G., Jenkin, M. E., Rossi, M. J., Troe, J. and IUPAC Subcommittee: Evaluated kinetic and photochemical data for atmospheric chemistry: Volume II - gas phase reactions of organic species, *Atmospheric Chem. Phys.*, 6(11), 3625–4055, doi:10.5194/acp-6-3625-2006, 2006.
- Baker, J. W. and Easty, D. M.: Hydrolysis of organic nitrates, *Nature*, 166(4212), 156–156, 1950.
- 500 Bateman, A. P., Nizkorodov, S. A., Laskin, J. and Laskin, A.: Photolytic processing of secondary organic aerosols dissolved in cloud droplets, *Phys. Chem. Chem. Phys.*, 13(26), 12199, doi:10.1039/c1cp20526a, 2011.
- Bean, J. K. and Hildebrandt Ruiz, L.: Gas–particle partitioning and hydrolysis of organic nitrates formed from the oxidation of  $\alpha$  -pinene in environmental chamber experiments, *Atmospheric Chem. Phys.*, 16(4), 2175–2184, doi:10.5194/acp-16-2175-2016, 2016.
- 505 Biesenthal, T. A., Wu, Q., Shepson, P. B., Wiebe, H. A., Anlauf, K. G. and Mackay, G. I.: A study of relationships between isoprene, its oxidation products, and ozone, in the Lower Fraser Valley, BC, *Atmos. Environ.*, 31(14), 2049–2058, doi:10.1016/S1352-2310(96)00318-4, 1997.
- Böge, O., Mutzel, A., Iinuma, Y., Yli-Pirilä, P., Kahnt, A., Joutsensaari, J. and Herrmann, H.: Gas-phase products and secondary organic aerosol formation from the ozonolysis and photooxidation of myrcene, *Atmos. Environ.*, 79, 553–560, doi:10.1016/j.atmosenv.2013.07.034, 2013.
- 510 Boyd, C. M., Sanchez, J., Xu, L., Eugene, A. J., Nah, T., Tuet, W. Y., Guzman, M. I. and Ng, N. L.: Secondary organic aerosol formation from the  $\beta$ -pinene+ $\text{NO}_3$  system: effect of humidity and peroxy radical fate, *Atmospheric Chem. Phys.*, 15(13), 7497–7522, doi:10.5194/acp-15-7497-2015, 2015.
- 515 Boyd, C. M., Nah, T., Xu, L., Berkemeier, T. and Ng, N. L.: Secondary Organic Aerosol (SOA) from Nitrate Radical Oxidation of Monoterpenes: Effects of Temperature, Dilution, and Humidity on Aerosol Formation, Mixing, and Evaporation, *Environ. Sci. Technol.*, 51(14), 7831–7841, doi: 10.1021/acs.est.7b01460, 2017.

- 520 Browne, E. C. and Cohen, R. C.: Effects of biogenic nitrate chemistry on the NO<sub>x</sub> lifetime in remote  
continental regions, *Atmospheric Chem. Phys.*, 12(24), 11917–11932, doi:10.5194/acp-12-11917-2012,  
2012.
- Budisulistiorini, S. H., Nenes, A., Carlton, A. G., Surratt, J. D., McNeill, V. F. and Pye, H. O. T.:  
525 Simulating Aqueous-Phase Isoprene-Epoxydiol (IEPOX) Secondary Organic Aerosol Production During  
the 2013 Southern Oxidant and Aerosol Study (SOAS), *Environ. Sci. Technol.*, 51(9), 5026–5034, doi:  
10.1021/acs.est.6b05750, 2017.
- Capouet, M., Peeters, J., Nozière, B. and Müller, J.-F.: Alpha-pinene oxidation by OH: simulations of  
laboratory experiments, *Atmospheric Chem. Phys.*, 4(9/10), 2285–2311, doi:10.5194/acp-4-2285-2004,  
2004.
- Carlton, A. G. and Turpin, B. J.: Particle partitioning potential of organic compounds is highest in the  
530 Eastern US and driven by anthropogenic water, *Atmospheric Chem. Phys.*, 13(20), 10203–10214,  
doi:10.5194/acp-13-10203-2013, 2013.
- Carrington, R. A. G.: The infra-red spectra of some organic nitrates, *Spectrochim. Acta*, 16(11–12), 1279–  
1293, 1960.
- Chen, X., Hulbert, D. and Shepson, P. B.: Measurement of the organic nitrate yield from OH reaction  
535 with isoprene, *J. Geophys. Res. Atmospheres*, 103(D19), 25563–25568, doi:10.1029/98JD01483, 1998.
- Darer, A. I., Cole-Filipiak, N. C., O'Connor, A. E. and Elrod, M. J.: Formation and Stability of  
Atmospherically Relevant Isoprene-Derived Organosulfates and Organonitrates, *Environ. Sci. Technol.*,  
45(5), 1895–1902, doi:10.1021/es103797z, 2011.
- Ditto, J. C., Joo, T., Slade, J. H., Shepson, P. B., Ng, N. L. and Gentner, D. R.: Nontargeted Tandem Mass  
540 Spectrometry Analysis Reveals Diversity and Variability in Aerosol Functional Groups across Multiple  
Sites, Seasons, and Times of Day, *Environ. Sci. Technol. Lett.*, 7(2), 60–69, doi:  
10.1021/acs.estlett.9b00702, 2020.
- Donahue, N. M., Epstein, S. A., Pandis, S. N. and Robinson, A. L.: A two-dimensional volatility basis  
set: 1. organic-aerosol mixing thermodynamics, *Atmospheric Chem. Phys.*, 11(7), 3303–3318,  
545 doi:10.5194/acp-11-3303-2011, 2011.
- Fisher, J. A., Jacob, D. J., Travis, K. R., Kim, P. S., Marais, E. A., Chan Miller, C., Yu, K., Zhu, L.,  
Yantosca, R. M., Sulprizio, M. P., Mao, J., Wennberg, P. O., Crouse, J. D., Teng, A. P., Nguyen, T. B.,  
St. Clair, J. M., Cohen, R. C., Romer, P., Nault, B. A., Wooldridge, P. J., Jimenez, J. L., Campuzano-Jost,  
P., Day, D. A., Hu, W., Shepson, P. B., Xiong, F., Blake, D. R., Goldstein, A. H., Misztal, P. K., Hanisco,  
550 T. F., Wolfe, G. M., Ryerson, T. B., Wisthaler, A. and Mikoviny, T.: Organic nitrate chemistry and its  
implications for nitrogen budgets in an isoprene- and monoterpene-rich atmosphere: constraints from

- aircraft (SEAC4RS) and ground-based (SOAS) observations in the Southeast US, *Atmospheric Chem. Phys.*, 16(9), 5969–5991, doi:10.5194/acp-16-5969-2016, 2016.
- 555 Fry, J. L., Kiendler-Scharr, A., Rollins, A. W., Wooldridge, P. J., Brown, S. S., Fuchs, H., Dube, W., Mensah, A., dal Maso, M., Tillmann, R., Dorn, H. P., Brauers, T. and Cohen, R. C.: Organic nitrate and secondary organic aerosol yield from NO<sub>3</sub> oxidation of beta-pinene evaluated using a gas-phase kinetics/aerosol partitioning model, *Atmospheric Chem. Phys.*, 9(4), 1431–1449, 2009.
- 560 Fry, J. L., Draper, D. C., Barsanti, K. C., Smith, J. N., Ortega, J., Winkler, P. M., Lawler, M. J., Brown, S. S., Edwards, P. M., Cohen, R. C. and Lee, L.: Secondary Organic Aerosol Formation and Organic Nitrate Yield from NO<sub>3</sub> Oxidation of Biogenic Hydrocarbons, *Environ. Sci. Technol.*, 48(20), 11944–11953, doi:10.1021/es502204x, 2014.
- Galbavy, E. S., Anastasio, C., Lefer, B. and Hall, S.: Light penetration in the snowpack at Summit, Greenland: Part 2 Nitrate photolysis, *Atmos. Environ.*, 41(24), 5091–5100, doi:10.1016/j.atmosenv.2006.01.066, 2007.
- 565 Gaona-Colmán, E., Blanco, M. B., Barnes, I., Wiesen, P. and Teruel, M. A.: Atmospheric sink of β-ocimene and camphene initiated by Cl atoms: kinetics and products at NO<sub>x</sub> free-air, *RSC Adv.*, 8(48), 27054–27063, doi:10.1039/C8RA04931A, 2018.
- Glasius, M. and Goldstein, A. H.: Recent Discoveries and Future Challenges in Atmospheric Organic Chemistry, *Environ. Sci. Technol.*, 50(6), 2754–2764, doi:10.1021/acs.est.5b05105, 2016.
- 570 Goldstein, A. H. and Galbally, I. E.: Known and Unexplored Organic Constituents in the Earth's Atmosphere, *Environ. Sci. Technol.*, 41(5), 1514–1521, doi:10.1021/es072476p, 2007.
- Griffin, R. J., Cocker, D. R., Seinfeld, J. H. and Dabdub, D.: Estimate of global atmospheric organic aerosol from oxidation of biogenic hydrocarbons, *Geophys. Res. Lett.*, 26(17), 2721–2724, doi:10.1029/1999GL900476, 1999.
- 575 Guenther, A., Hewitt, C. N., Erickson, D., Fall, R., Geron, C., Graedel, T., Harley, P., Klinger, L., Lerdau, M., Mckay, W. A., Pierce, T., Scholes, B., Steinbrecher, R., Tallamraju, R., Taylor, J. and Zimmerman, P.: A global model of natural volatile organic compound emissions, *J. Geophys. Res.*, 100(D5), 8873, doi:10.1029/94JD02950, 1995.
- 580 Guenther, A. B., Jiang, X., Heald, C. L., Sakulyanontvittaya, T., Duhl, T., Emmons, L. K. and Wang, X.: The Model of Emissions of Gases and Aerosols from Nature version 2.1 (MEGAN2.1): an extended and updated framework for modeling biogenic emissions, *Geosci Model Dev*, 5(6), 1471–1492, doi:10.5194/gmd-5-1471-2012, 2012.
- Hallquist, M., Wenger, J. C., Baltensperger, U., Rudich, Y., Simpson, D., Claeys, M., Dommen, J., Donahue, N. M., George, C., Goldstein, A. H., Hamilton, J. F., Herrmann, H., Hoffmann, T., Iinuma, Y.,

- 585 Jang, M., Jenkin, M. E., Jimenez, J. L., Kiendler-Scharr, A., Maenhaut, W., McFiggans, G., Mentel, Th. F., Monod, A., Prévôt, A. S. H., Seinfeld, J. H., Surratt, J. D., Szmigielski, R. and Wildt, J.: The formation, properties and impact of secondary organic aerosol: current and emerging issues, *Atmospheric Chem. Phys.*, 9(14), 5155–5236, doi:10.5194/acp-9-5155-2009, 2009.
- Hatakeyama, S., Izumi, K., Fukuyama, T., Akimoto, H. and Washida, N.: Reactions of OH with  $\alpha$ -pinene  
590 and  $\beta$ -pinene in air: Estimate of global CO production from the atmospheric oxidation of terpenes, *J. Geophys. Res.*, 96(D1), 947, doi:10.1029/90JD02341, 1991.
- Heinritzi, M., Dada, L., Simon, M., Stolzenburg, D., Wagner, A. C., Fischer, L., Ahonen, L. R., Amanatidis, S., Baalbaki, R., Baccharini, A., Bauer, P. S., Baumgartner, B., Bianchi, F., Brilke, S., Chen, D., Chiu, R., Dias, A., Dommen, J., Duplissy, J., Finkenzeller, H., Frege, C., Fuchs, C., Garmash, O.,  
595 Gordon, H., Granzin, M., Haddad, I. E., He, X., Helm, J., Hofbauer, V., Hoyle, C. R., Kangasluoma, J., Keber, T., Kim, C., Kürten, A., Lamkaddam, H., Lampilahti, J., Laurila, T. M., Lee, C. P., Lehtipalo, K., Leiminger, M., Mai, H., Makhmutov, V., Manninen, H. E., Marten, R., Mathot, S., Mauldin, R. L., Mentler, B., Molteni, U., Müller, T., Nie, W., Nieminen, T., Onnela, A., Partoll, E., Passananti, M., Petäjä, T., Pfeifer, J., Pospisilova, V., Quéléver, L., Rissanen, M. P., Rose, C., Schobesberger, S., Scholz, W.,  
600 Scholze, K., Sipilä, M., Steiner, G., Stozhkov, Y., Tauber, C., Tham, Y. J., Vazquez-Pufleau, M., Virtanen, A., Vogel, A. L., Volkamer, R., Wagner, R., Wang, M., Weitz, L., Wimmer, D., Xiao, M., Yan, C., Ye, P., Zha, Q., Zhou, X., Amorim, A., Baltensperger, U., Hansel, A., Kulmala, M., Tomé, A., Winkler, P. M., Worsnop, D. R., Donahue, N. M., Kirkby, J. and Curtius, J.: Molecular understanding of the suppression of new-particleformation by isoprene, preprint, *Aerosols/Laboratory Studies/Troposphere/Chemistry (chemical composition and reactions)*., 2020.  
605
- Hoffmann, T., Odum, J. R., Bowman, F., Collins, D., Klockow, D., Flagan, R. C. and Seinfeld, J. H.: Formation of Organic Aerosols from the Oxidation of Biogenic Hydrocarbons, *J. Atmospheric Chem.*, 26(2), 189–222, doi:10.1023/A:1005734301837, 1997.
- Hu, K. S., Darer, A. I. and Elrod, M. J.: Thermodynamics and kinetics of the hydrolysis of atmospherically  
610 relevant organonitrates and organosulfates, *Atmospheric Chem. Phys.*, 11(16), 8307–8320, doi:10.5194/acp-11-8307-2011, 2011.
- Isaksen, I. S. A., Granier, C., Myhre, G., Berntsen, T. K., Dalsøren, S. B., Gauss, M., Klimont, Z., Benestad, R., Bousquet, P., Collins, W., Cox, T., Eyring, V., Fowler, D., Fuzzi, S., Jöckel, P., Laj, P., Lohmann, U., Maione, M., Monks, P., Prevot, A. S. H., Raes, F., Richter, A., Rognerud, B., Schulz, M.,  
615 Shindell, D., Stevenson, D. S., Storelvmo, T., Wang, W.-C., van Weele, M., Wild, M. and Wuebbles, D.: Atmospheric composition change: Climate–Chemistry interactions, *Atmos. Environ.*, 43(33), 5138–5192, doi:10.1016/j.atmosenv.2009.08.003, 2009.
- Iyer, S., Lopez-Hilfiker, F., Lee, B. H., Thornton, J. A. and Kurtén, T.: Modeling the Detection of Organic and Inorganic Compounds Using Iodide-Based Chemical Ionization, *J. Phys. Chem. A*, 120(4), 576–587,  
620 doi: 10.1021/acs.jpca.5b09837, 2016.

- Jacobs, M. I., Burke, W. J. and Elrod, M. J.: Kinetics of the reactions of isoprene-derived hydroxynitrates: gas phase epoxide formation and solution phase hydrolysis, *Atmospheric Chem. Phys.*, 14(17), 8933–8946, doi:10.5194/acp-14-8933-2014, 2014.
- 625 Kwok, E. and Atkinson, R.: Estimation of hydroxyl radical reaction rate constants for gas-phase organic compounds using a structure-reactivity relationship: An update, *Atmos. Environ.*, 29(14), 1685–1695, doi:10.1016/1352-2310(95)00069-B, 1995.
- Lee, A., Goldstein, A. H., Kroll, J. H., Ng, N. L., Varutbangkul, V., Flagan, R. C. and Seinfeld, J. H.: Gas-phase products and secondary aerosol yields from the photooxidation of 16 different terpenes, *J. Geophys. Res.*, 111(D17), doi:10.1029/2006JD007050, 2006.
- 630 Lee, B. H., Mohr, C., Lopez-Hilfiker, F. D., Lutz, A., Hallquist, M., Lee, L., Romer, P., Cohen, R. C., Iyer, S., Kurtén, T., Hu, W., Day, D. A., Campuzano-Jost, P., Jimenez, J. L., Xu, L., Ng, N. L., Guo, H., Weber, R. J., Wild, R. J., Brown, S. S., Koss, A., de Gouw, J., Olson, K., Goldstein, A. H., Seco, R., Kim, S., McAvey, K., Shepson, P. B., Starn, T., Baumann, K., Edgerton, E. S., Liu, J., Shilling, J. E., Miller, D. O., Brune, W., Schobesberger, S., D'Ambro, E. L. and Thornton, J. A.: Highly functionalized organic  
635 nitrates in the southeast United States: Contribution to secondary organic aerosol and reactive nitrogen budgets, *Proc. Natl. Acad. Sci.*, 113(6), 1516–1521, doi:10.1073/pnas.1508108113, 2016.
- Liu, S., Shilling, J. E., Song, C., Hiranuma, N., Zaveri, R. A. and Russell, L. M.: Hydrolysis of Organonitrate Functional Groups in Aerosol Particles, *Aerosol Sci. Technol.*, 46(12), 1359–1369, doi:10.1080/02786826.2012.716175, 2012.
- 640 Liu, T., Clegg, S. L. and Abbatt, J. P. D.: Fast oxidation of sulfur dioxide by hydrogen peroxide in deliquesced aerosol particles, *Proc. Natl. Acad. Sci.*, 117(3), 1354–1359, doi:10.1073/pnas.1916401117, 2020.
- Lockwood, A. L., Shepson, P. B., Fiddler, M. N. and Alaghmand, M.: Isoprene nitrates: preparation, separation, identification, yields, and atmospheric chemistry, *Atmospheric Chem. Phys.*, 10(13), 6169–  
645 6178, doi:10.5194/acp-10-6169-2010, 2010.
- Lopez-Hilfiker, F. D., Iyer, S., Mohr, C., Lee, B. H., D'Ambro, E. L., Kurtén, T. and Thornton, J. A.: Constraining the sensitivity of iodide adduct chemical ionization mass spectrometry to multifunctional organic molecules using the collision limit and thermodynamic stability of iodide ion adducts, *Atmospheric Meas. Tech.*, 9(4), 1505–1512, doi:10.5194/amt-9-1505-2016, 2016.
- 650 Monks, P. S., Granier, C., Fuzzi, S., Stohl, A., Williams, M. L., Akimoto, H., Amann, M., Baklanov, A., Baltensperger, U., Bey, I., Blake, N., Blake, R. S., Carslaw, K., Cooper, O. R., Dentener, F., Fowler, D., Fragkou, E., Frost, G. J., Generoso, S., Ginoux, P., Grewe, V., Guenther, A., Hansson, H. C., Henne, S., Hjorth, J., Hofzumahaus, A., Huntrieser, H., Isaksen, I. S. A., Jenkin, M. E., Kaiser, J., Kanakidou, M., Klimont, Z., Kulmala, M., Laj, P., Lawrence, M. G., Lee, J. D., Lioussse, C., Maione, M., McFiggans, G.,  
655 Metzger, A., Mieville, A., Moussiopoulos, N., Orlando, J. J., O'Dowd, C. D., Palmer, P. I., Parrish, D.

- D., Petzold, A., Platt, U., Pöschl, U., Prévôt, A. S. H., Reeves, C. E., Reimann, S., Rudich, Y., Sellegri, K., Steinbrecher, R., Simpson, D., ten Brink, H., Theloke, J., van der Werf, G. R., Vautard, R., Vestreng, V., Vlachokostas, Ch. and von Glasow, R.: Atmospheric composition change – global and regional air quality, *Atmos. Environ.*, 43(33), 5268–5350, doi:10.1016/j.atmosenv.2009.08.021, 2009.
- 660 Ng, N. L., Kroll, J. H., Keywood, M. D., Bahreini, R., Varutbangkul, V., Flagan, R. C., Seinfeld, J. H., Lee, A. and Goldstein, A. H.: Contribution of First- versus Second-Generation Products to Secondary Organic Aerosols Formed in the Oxidation of Biogenic Hydrocarbons, *Environ. Sci. Technol.*, 40(7), 2283–2297, doi:10.1021/es052269u, 2006.
- 665 Ng, N. L., Brown, S. S., Archibald, A. T., Atlas, E., Cohen, R. C., Crowley, J. N., Day, D. A., Donahue, N. M., Fry, J. L., Fuchs, H., Griffin, R. J., Guzman, M. I., Herrmann, H., Hodzic, A., Iinuma, Y., Jimenez, J. L., Kiendler-Scharr, A., Lee, B. H., Luecken, D. J., Mao, J., McLaren, R., Mutzel, A., Osthoff, H. D., Ouyang, B., Picquet-Varrault, B., Platt, U., Pye, H. O. T., Rudich, Y., Schwantes, R. H., Shiraiwa, M., Stutz, J., Thornton, J. A., Tilgner, A., Williams, B. J. and Zaveri, R. A.: Nitrate radicals and biogenic volatile organic compounds: oxidation, mechanisms, and organic aerosol, *Atmospheric Chem. Phys.*, 670 17(3), 2103–2162, doi:10.5194/acp-17-2103-2017, 2017.
- Nielsen, T., Egeløv, A. H., Granby, K. and Skov, H.: Observations on particulate organic nitrates and unidentified components of NO<sub>y</sub>, *Atmos. Environ.*, 29(15), 1757–1769, doi:10.1016/1352-2310(95)00098-J, 1995.
- 675 Otto, T., Stieger, B., Mettke, P. and Herrmann, H.: Tropospheric Aqueous-Phase Oxidation of Isoprene-Derived Dihydroxycarbonyl Compounds, *J. Phys. Chem. A*, 121(34), 6460–6470, doi:10.1021/acs.jpca.7b05879, 2017.
- Pankow, J. F. and Asher, W. E.: SIMPOL.1: a simple group contribution method for predicting vapor pressures and enthalpies of vaporization of multifunctional organic compounds, *Atmospheric Chem. Phys.*, 8(10), 2773–2796, doi:10.5194/acp-8-2773-2008, 2008.
- 680 Perraud, V., Bruns, E. A., Ezell, M. J., Johnson, S. N., Yu, Y., Alexander, M. L., Zelenyuk, A., Imre, D., Chang, W. L., Dabdub, D., Pankow, J. F. and Finlayson-Pitts, B. J.: Nonequilibrium atmospheric secondary organic aerosol formation and growth, *Proc. Natl. Acad. Sci.*, 109(8), 2836–2841, doi:10.1073/pnas.1119909109, 2012.
- 685 Perring, A. E., Pusede, S. E. and Cohen, R. C.: An Observational Perspective on the Atmospheric Impacts of Alkyl and Multifunctional Nitrates on Ozone and Secondary Organic Aerosol, *Chem. Rev.*, 113(8), 5848–5870, doi:10.1021/cr300520x, 2013.
- Possanzini, M., Palo, V. D. and Cecinato, A.: Sources and photodecomposition of formaldehyde and acetaldehyde in Rome ambient air, *Atmos. Environ.*, 36(19), 3195–3201, doi:10.1016/S1352-2310(02)00192-9, 2002.

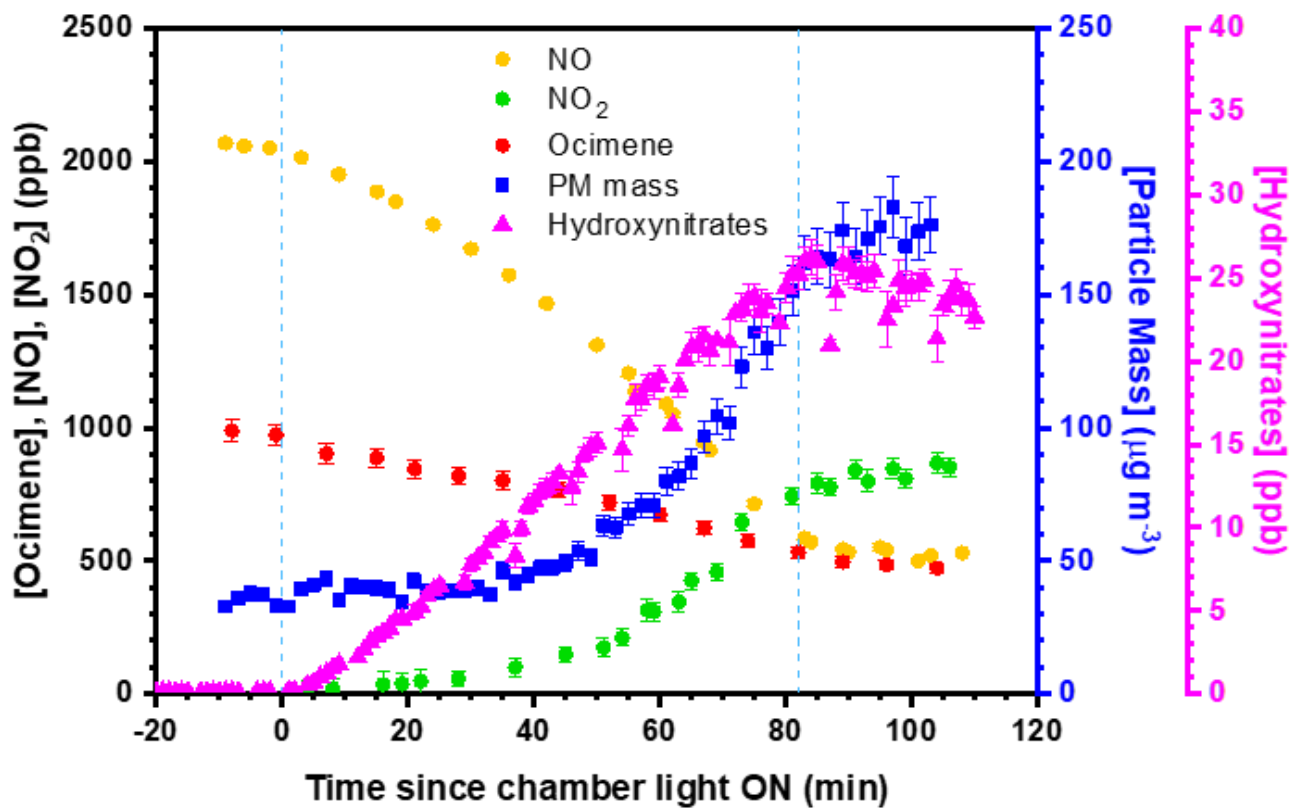


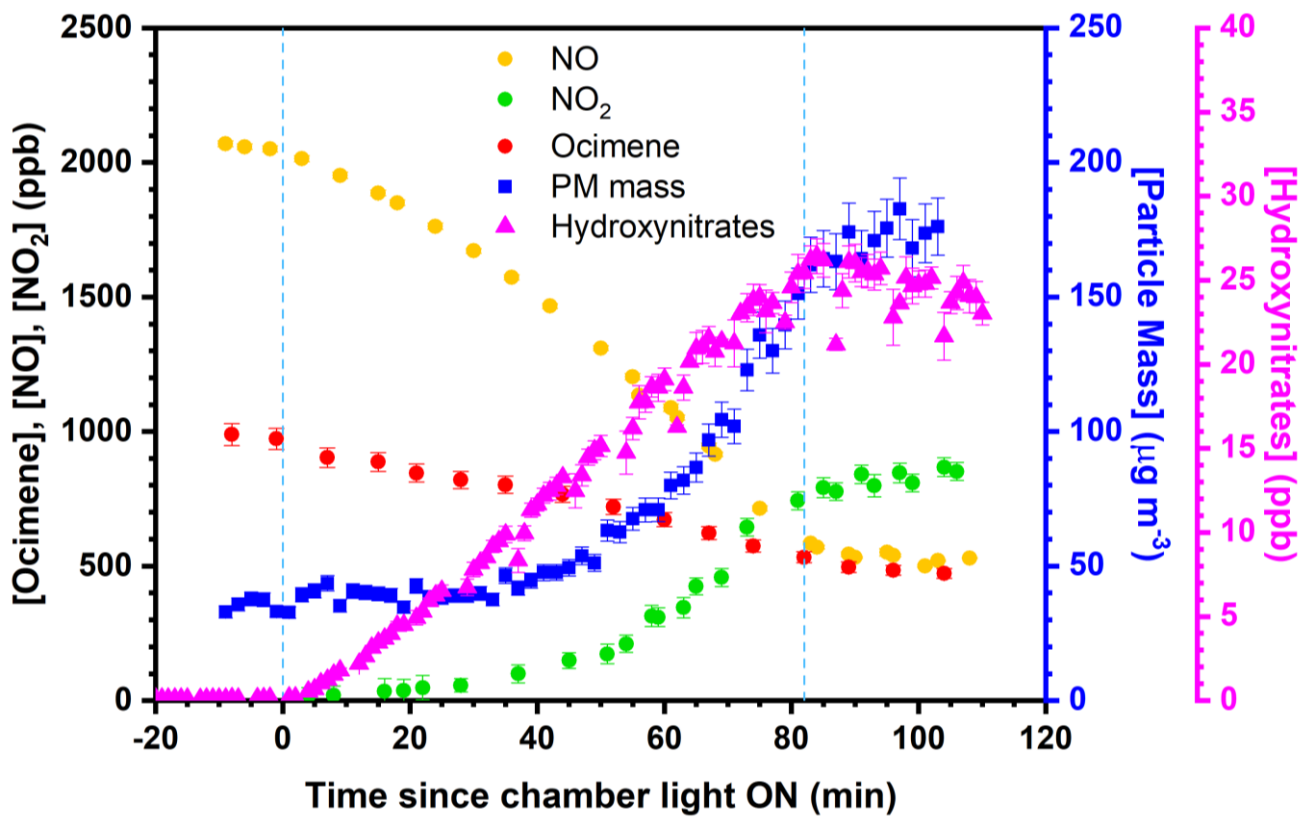
- 690 Pratt, K. A., Mielke, L. H., Shepson, P. B., Bryan, A. M., Steiner, A. L., Ortega, J., Daly, R., Helmig, D., Vogel, C. S., Griffith, S., Dusanter, S., Stevens, P. S. and Alaghmand, M.: Contributions of individual reactive biogenic volatile organic compounds to organic nitrates above a mixed forest, *Atmospheric Chem. Phys.*, 12(21), 10125–10143, doi:10.5194/acp-12-10125-2012, 2012.
- Pusede, S. E., Steiner, A. L. and Cohen, R. C.: Temperature and Recent Trends in the Chemistry of  
695 Continental Surface Ozone, *Chem. Rev.*, 115(10), 3898–3918, doi:10.1021/cr5006815, 2015.
- Pye, H. O. T., Pinder, R. W., Piletic, I. R., Xie, Y., Capps, S. L., Lin, Y.-H., Surratt, J. D., Zhang, Z., Gold, A., Luecken, D. J., Hutzell, W. T., Jaoui, M., Offenberg, J. H., Kleindienst, T. E., Lewandowski, M. and Edney, E. O.: Epoxide Pathways Improve Model Predictions of Isoprene Markers and Reveal Key Role of Acidity in Aerosol Formation, *Environ. Sci. Technol.*, 47(19), 11056–11064,  
700 doi:10.1021/es402106h, 2013.
- Pye, H. O. T., Luecken, D. J., Xu, L., Boyd, C. M., Ng, N. L., Baker, K. R., Ayres, B. R., Bash, J. O., Baumann, K., Carter, W. P. L., Edgerton, E., Fry, J. L., Hutzell, W. T., Schwede, D. B. and Shepson, P. B.: Modeling the Current and Future Roles of Particulate Organic Nitrates in the Southeastern United States, *Environ. Sci. Technol.*, 49(24), 14195–14203, doi: 10.1021/acs.est.5b03738, 2015.
- 705 Reissell, A.: Products of the OH radical- and O<sub>3</sub>-initiated reactions of myrcene and ocimene, *J. Geophys. Res.*, 107(D12), 4138, doi:10.1029/2001JD001234, 2002.
- Rindelaub, J. D., McAvey, K. M. and Shepson, P. B.: The photochemical production of organic nitrates from  $\alpha$ -pinene and loss via acid-dependent particle phase hydrolysis, *Atmos. Environ.*, 100, 193–201, doi: 10.1016/j.atmosenv.2014.11.010, 2015.
- 710 Rindelaub, J. D., Wiley, J. S., Cooper, B. R. and Shepson, P. B.: Chemical characterization of  $\alpha$ -pinene secondary organic aerosol constituents using gas chromatography, liquid chromatography, and paper spray-based mass spectrometry techniques: Characterization of  $\alpha$ -pinene SOA constituents, *Rapid Commun. Mass Spectrom.*, 30(13), 1627–1638, doi:10.1002/rcm.7602, 2016a.
- Rindelaub, J. D., Borca, C. H., Hostetler, M. A., Slade, J. H., Lipton, M. A., Slipchenko, L. V. and  
715 Shepson, P. B.: The acid-catalyzed hydrolysis of an  $\alpha$ -pinene-derived organic nitrate: kinetics, products, reaction mechanisms, and atmospheric impact, *Atmospheric Chem. Phys.*, 16(23), 15425–15432, doi:10.5194/acp-16-15425-2016, 2016b.
- Rollins, A. W., Browne, E. C., Min, K.-E., Pusede, S. E., Wooldridge, P. J., Gentner, D. R., Goldstein, A. H., Liu, S., Day, D. A., Russell, L. M. and Cohen, R. C.: Evidence for NO<sub>x</sub> Control over Nighttime  
720 SOA Formation, *Science*, 337(6099), 1210–1212, doi:10.1126/science.1221520, 2012.
- Rollins, A. W., Pusede, S., Wooldridge, P., Min, K.-E., Gentner, D. R., Goldstein, A. H., Liu, S., Day, D. A., Russell, L. M., Rubitschun, C. L., Surratt, J. D. and Cohen, R. C.: Gas/particle partitioning of total

- alkyl nitrates observed with TD-LIF in Bakersfield: RONO<sub>2</sub> PHASE PARTITIONING, *J. Geophys. Res. Atmospheres*, 118(12), 6651–6662, doi:10.1002/jgrd.50522, 2013.
- 725 Romer, P. S., Duffey, K. C., Wooldridge, P. J., Allen, H. M., Ayres, B. R., Brown, S. S., Brune, W. H., Crouse, J. D., De Gouw, J. and Draper, D. C.: The lifetime of nitrogen oxides in an isoprene-dominated forest, *Atmospheric Chem. Phys.*, 16(12), 7623–7637, 2016.
- Romer Present, P. S., Zare, A. and Cohen, R. C.: The changing role of organic nitrates in the removal and transport of NO<sub>x</sub>, preprint, *Gases/Field Measurements/Troposphere/Chemistry (chemical composition and reactions)*., 2019.
- 730 Schulze, B. C., Wallace, H. W., Flynn, J. H., Lefer, B. L., Erickson, M. H., Jobson, B. T., Dusanter, S., Griffith, S. M., Hansen, R. F., Stevens, P. S., VanReken, T. and Griffin, R. J.: Differences in BVOC oxidation and SOA formation above and below the forest canopy, *Atmospheric Chem. Phys.*, 17(3), 1805–1828, doi:10.5194/acp-17-1805-2017, 2017.
- 735 Seinfeld, J. H. and Pandis, S. N.: Chapter 14 | Atmospheric Organic Aerosols, in *Atmospheric chemistry and physics: from air pollution to climate change*, pp. 573–660, John Wiley & Sons, Hoboken, New Jersey., 2016.
- Shepson, P. B., Mackay, E. and Muthuramu, K.: Henry’s Law Constants and Removal Processes for Several Atmospheric  $\beta$ -Hydroxy Alkyl Nitrates, *Environ. Sci. Technol.*, 30(12), 3618–3623, doi:10.1021/es960538y, 1996.
- 740 Slade, J. H., de Perre, C., Lee, L. and Shepson, P. B.: Nitrate radical oxidation of  $\gamma$ -terpinene: hydroxy nitrate, total organic nitrate, and secondary organic aerosol yields, *Atmospheric Chem. Phys.*, 17(14), 8635–8650, doi:10.5194/acp-17-8635-2017, 2017.
- Slade, J. H., Ault, A. P., Bui, A. T., Ditto, J. C., Lei, Z., Bondy, A. L., Olson, N. E., Cook, R. D., Desrochers, S. J., Harvey, R. M., Erickson, M. H., Wallace, H. W., Alvarez, S. L., Flynn, J. H., Boor, B. E., Petrucci, G. A., Gentner, D. R., Griffin, R. J. and Shepson, P. B.: Bouncer Particles at Night: Biogenic Secondary Organic Aerosol Chemistry and Sulfate Drive Diel Variations in the Aerosol Phase in a Mixed Forest, *Environ. Sci. Technol.*, 53(9), 4977–4987, doi: 10.1021/acs.est.8b07319, 2019.
- 745 Stropoli, S. J., Miner, C. R., Hill, D. R. and Elrod, M. J.: Assessing Potential Oligomerization Reaction Mechanisms of Isoprene Epoxydiols on Secondary Organic Aerosol, *Environ. Sci. Technol.*, 53(1), 176–184, doi: 10.1021/acs.est.8b05247, 2019.
- Suarez-Bertoa, R., Picquet-Varrault, B., Tamas, W., Pangui, E. and Doussin, J.-F.: Atmospheric Fate of a Series of Carbonyl Nitrates: Photolysis Frequencies and OH-Oxidation Rate Constants, *Environ. Sci. Technol.*, 46(22), 12502–12509, doi:10.1021/es302613x, 2012.

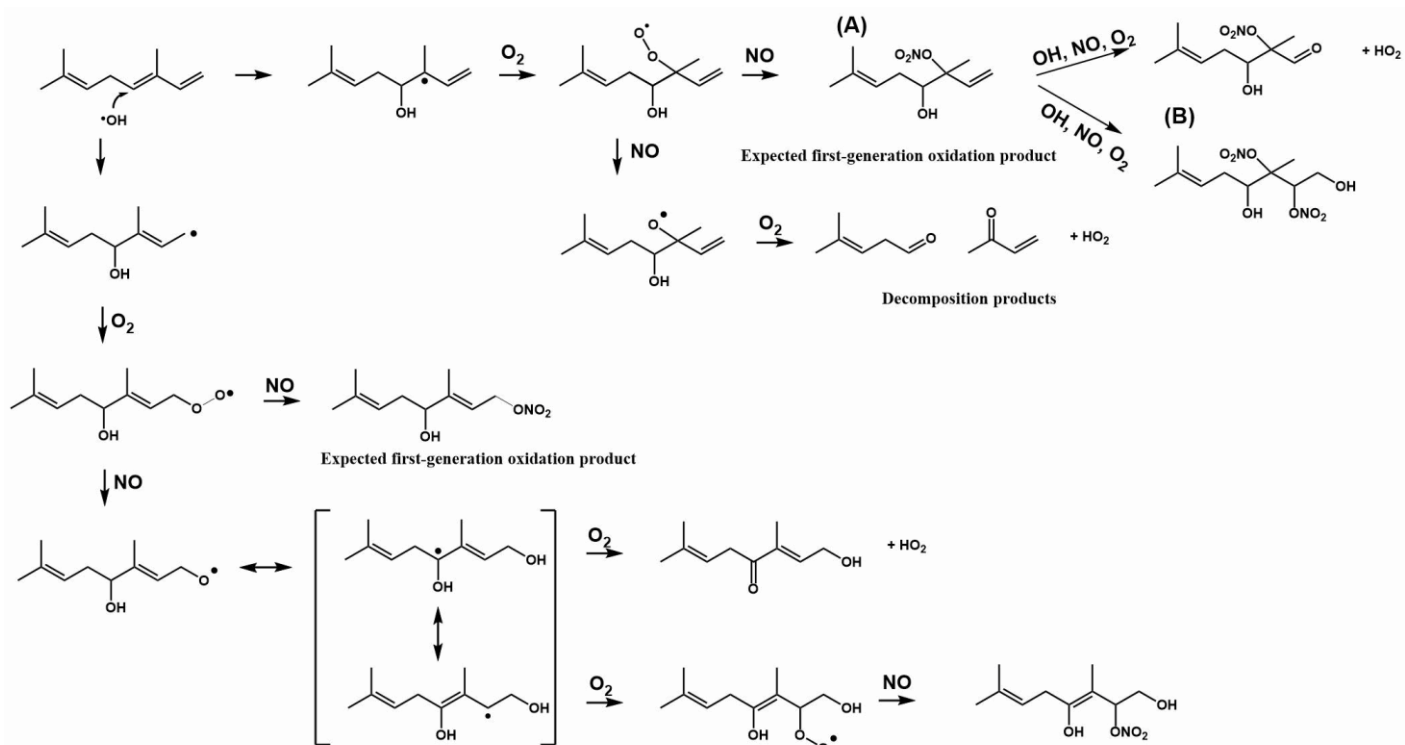
- 755 Surratt, J. D., Kroll, J. H., Kleindienst, T. E., Edney, E. O., Claeys, M., Sorooshian, A., Ng, N. L., Offenberg, J. H., Lewandowski, M., Jaoui, M., Flagan, R. C. and Seinfeld, J. H.: Evidence for Organosulfates in Secondary Organic Aerosol, *Environ. Sci. Technol.*, 41(2), 517–527, doi:10.1021/es062081q, 2007.
- 760 Surratt, J. D., Gómez-González, Y., Chan, A. W. H., Vermeylen, R., Shahgholi, M., Kleindienst, T. E., Edney, E. O., Offenberg, J. H., Lewandowski, M., Jaoui, M., Maenhaut, W., Claeys, M., Flagan, R. C. and Seinfeld, J. H.: Organosulfate Formation in Biogenic Secondary Organic Aerosol, *J. Phys. Chem. A*, 112(36), 8345–8378, doi:10.1021/jp802310p, 2008.
- 765 Takeuchi, M. and Ng, N. L.: Chemical composition and hydrolysis of organic nitrate aerosol formed from hydroxyl and nitrate radical oxidation of  $\alpha$ -pinene and  $\beta$ -pinene, *Atmospheric Chem. Phys.*, 19(19), 12749–12766, doi:10.5194/acp-19-12749-2019, 2019.
- Teng, A. P., Crounse, J. D., Lee, L., St. Clair, J. M., Cohen, R. C. and Wennberg, P. O.: Hydroxy nitrate production in the OH-initiated oxidation of alkenes, *Atmospheric Chem. Phys.*, 15(8), 4297–4316, doi:10.5194/acp-15-4297-2015, 2015.
- 770 Teng, A. P., Crounse, J. D. and Wennberg, P. O.: Isoprene Peroxy Radical Dynamics, *J. Am. Chem. Soc.*, 139(15), 5367–5377, doi:10.1021/jacs.6b12838, 2017.
- Tsigaridis, K. and Kanakidou, M.: Secondary organic aerosol importance in the future atmosphere, *Atmos. Environ.*, 41(22), 4682–4692, doi: 10.1016/j.atmosenv.2007.03.045, 2007.
- Tuazon, E. C. and Atkinson, R.: A product study of the gas-phase reaction of isoprene with the OH radical in the presence of NO<sub>x</sub>, *Int. J. Chem. Kinet.*, 22(12), 1221–1236, 1990.
- 775 Walker, R. D. and Hawkins, J. E.: The Ultraviolet Absorption Spectra of Some Terpene Hydrocarbons, *J. Am. Chem. Soc.*, 74(16), 4209–4210, doi:10.1021/ja01136a512, 1952.
- 780 Xiong, F., McAvey, K. M., Pratt, K. A., Groff, C. J., Hostetler, M. A., Lipton, M. A., Starn, T. K., Seeley, J. V., Bertman, S. B., Teng, A. P., Crounse, J. D., Nguyen, T. B., Wennberg, P. O., Misztal, P. K., Goldstein, A. H., Guenther, A. B., Koss, A. R., Olson, K. F., de Gouw, J. A., Baumann, K., Edgerton, E. S., Feiner, P. A., Zhang, L., Miller, D. O., Brune, W. H. and Shepson, P. B.: Observation of isoprene hydroxynitrates in the southeastern United States and implications for the fate of NO<sub>x</sub>, *Atmos Chem Phys*, 15(19), 11257–11272, doi:10.5194/acp-15-11257-2015, 2015.
- 785 Xiong, F., Borca, C. H., Slipchenko, L. V. and Shepson, P. B.: Photochemical degradation of isoprene-derived 4,1-nitrooxy enal, *Atmospheric Chem. Phys.*, 16(9), 5595–5610, doi:10.5194/acp-16-5595-2016, 2016.
- Zafiriou, O. C. and True, M. B.: Nitrate photolysis in seawater by sunlight, *Mar. Chem.*, 8(1), 33–42, doi:10.1016/0304-4203(79)90030-6, 1979.

Zare, A., Romer, P. S., Nguyen, T., Keutsch, F. N., Skog, K. and Cohen, R. C.: A comprehensive organic nitrate chemistry: insights into the lifetime of atmospheric organic nitrates, *Atmospheric Chem. Phys.*, 18(20), 15419–15436, doi:10.5194/acp-18-15419-2018, 2018.





800 **Figure 1: Time series of  $\beta$ -ocimene oxidation and particle formation for experiment #6. Measurements presented are representative of all online measurements obtained during chamber experiments. The error bars represent the propagated analytical uncertainty and blue dashed lines represent the time of UV light irradiation. (PM = particulate matter).**



805

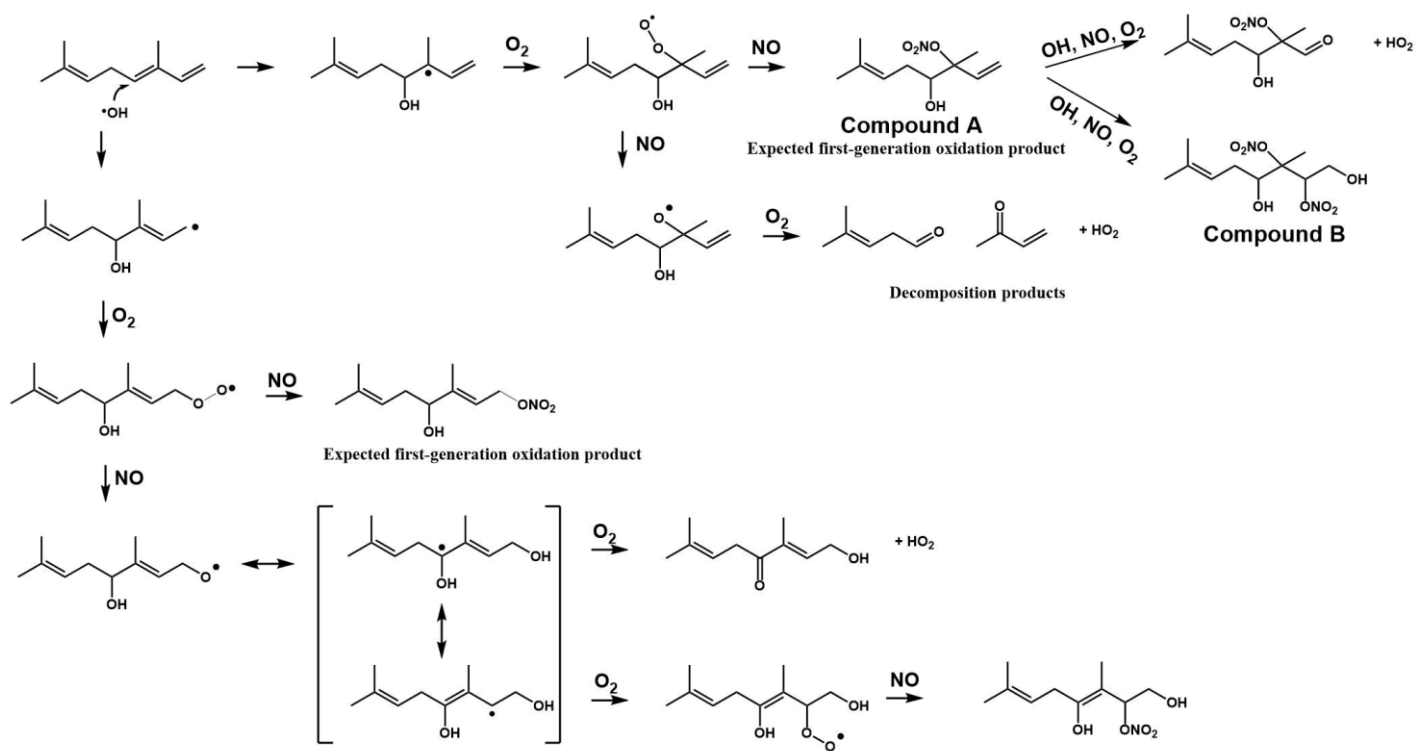
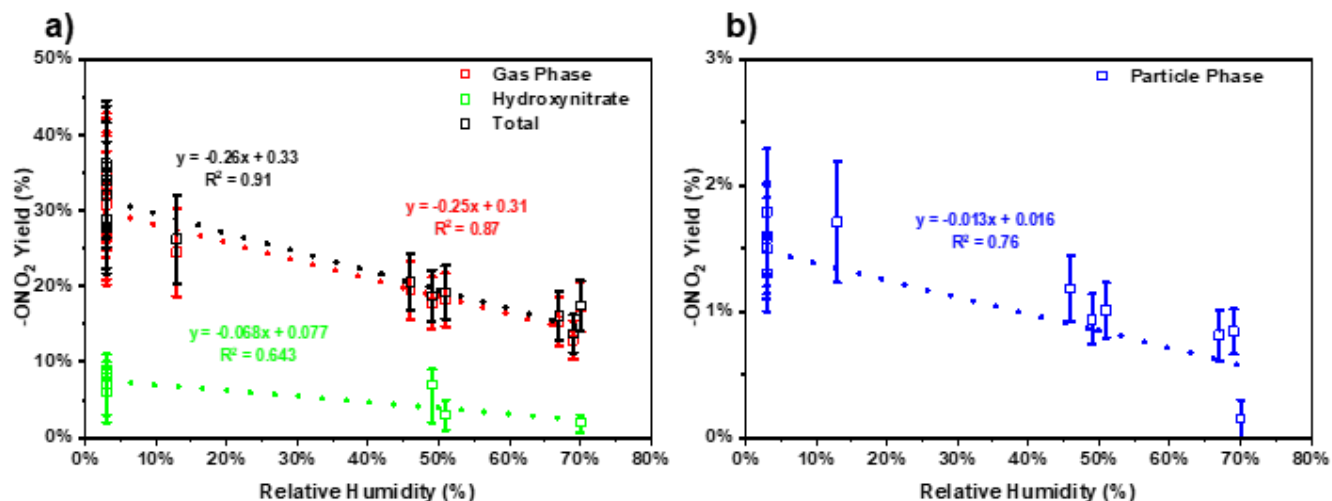


Figure 2: Example reaction pathways of the OH-initiated oxidation of  $\beta$ -ocimene in the presence of  $\text{NO}_x$ .

810



815

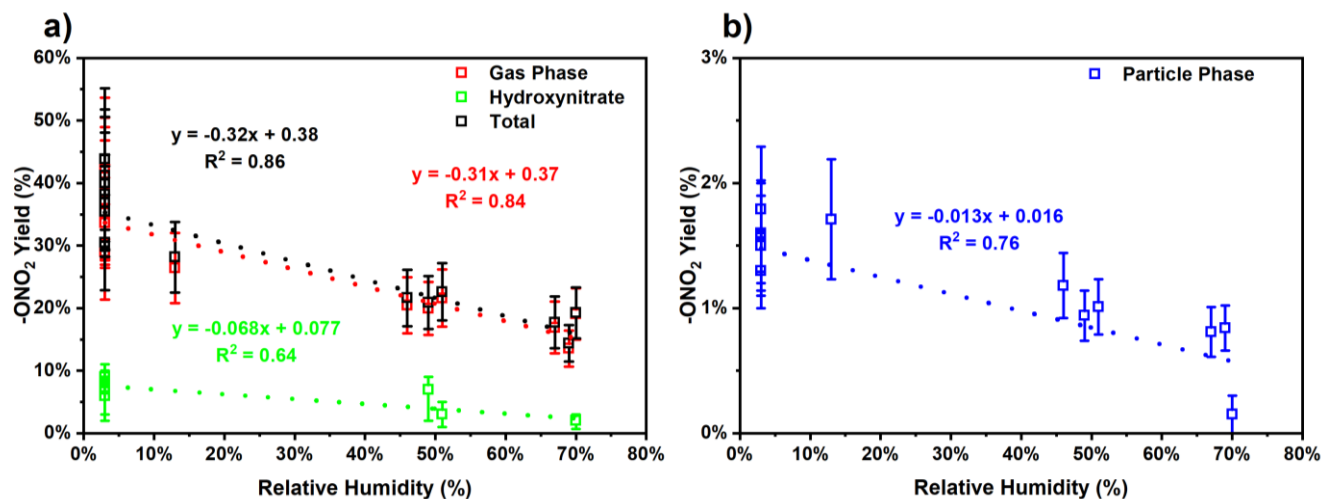
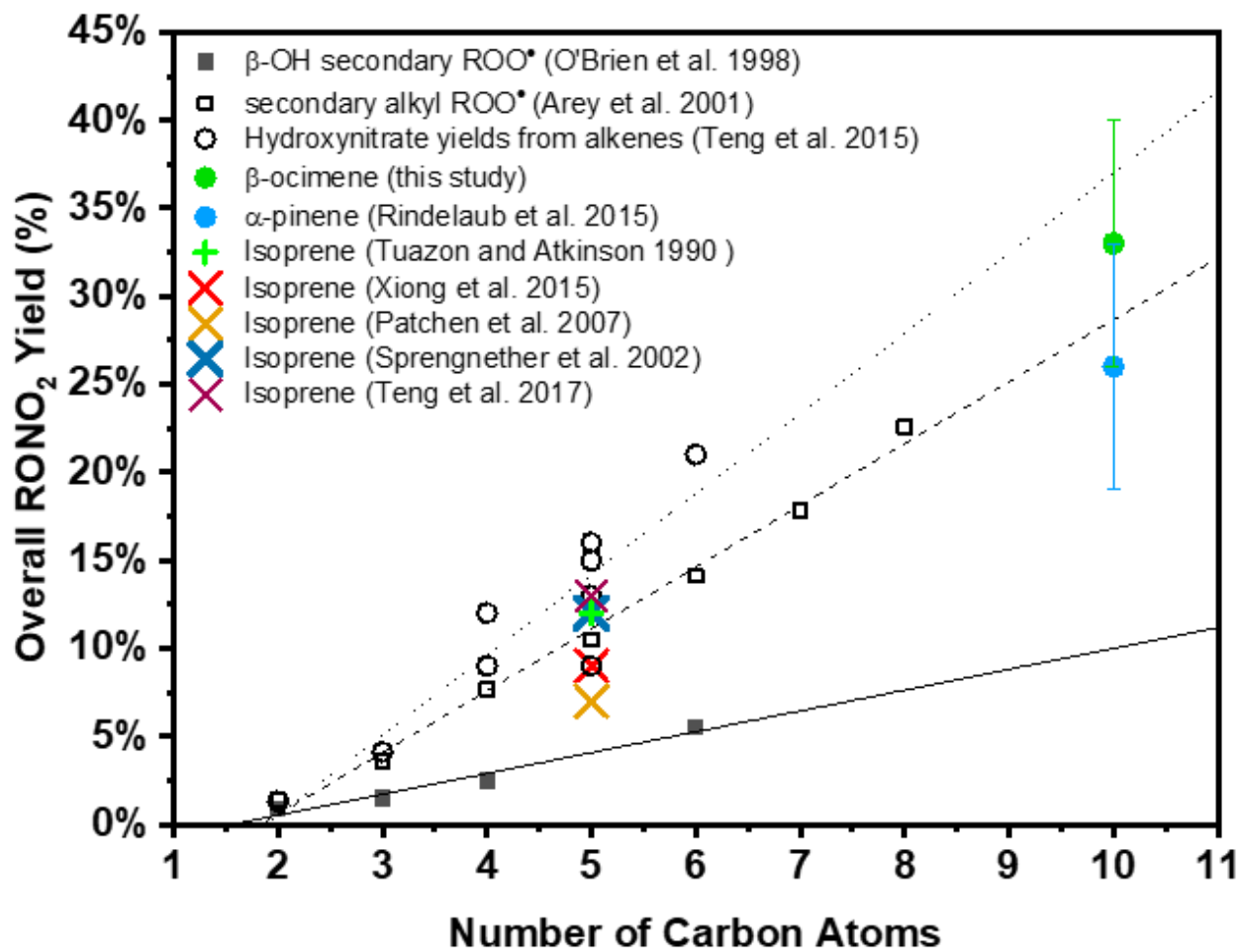


Figure 3: a) Wall-loss and dilution-corrected, total gas-phase organic nitrate ( $-\text{ONO}_2$ ), total (both gas- and particle-phase) organic nitrate (quantified by FTIR) and hydroxynitrate (quantified by CIMS) yield at different RH. b) Wall-loss and dilution-corrected, total particle-phase organic nitrate yield at different RH. Error bars represent the propagated analytical uncertainty of the yields.





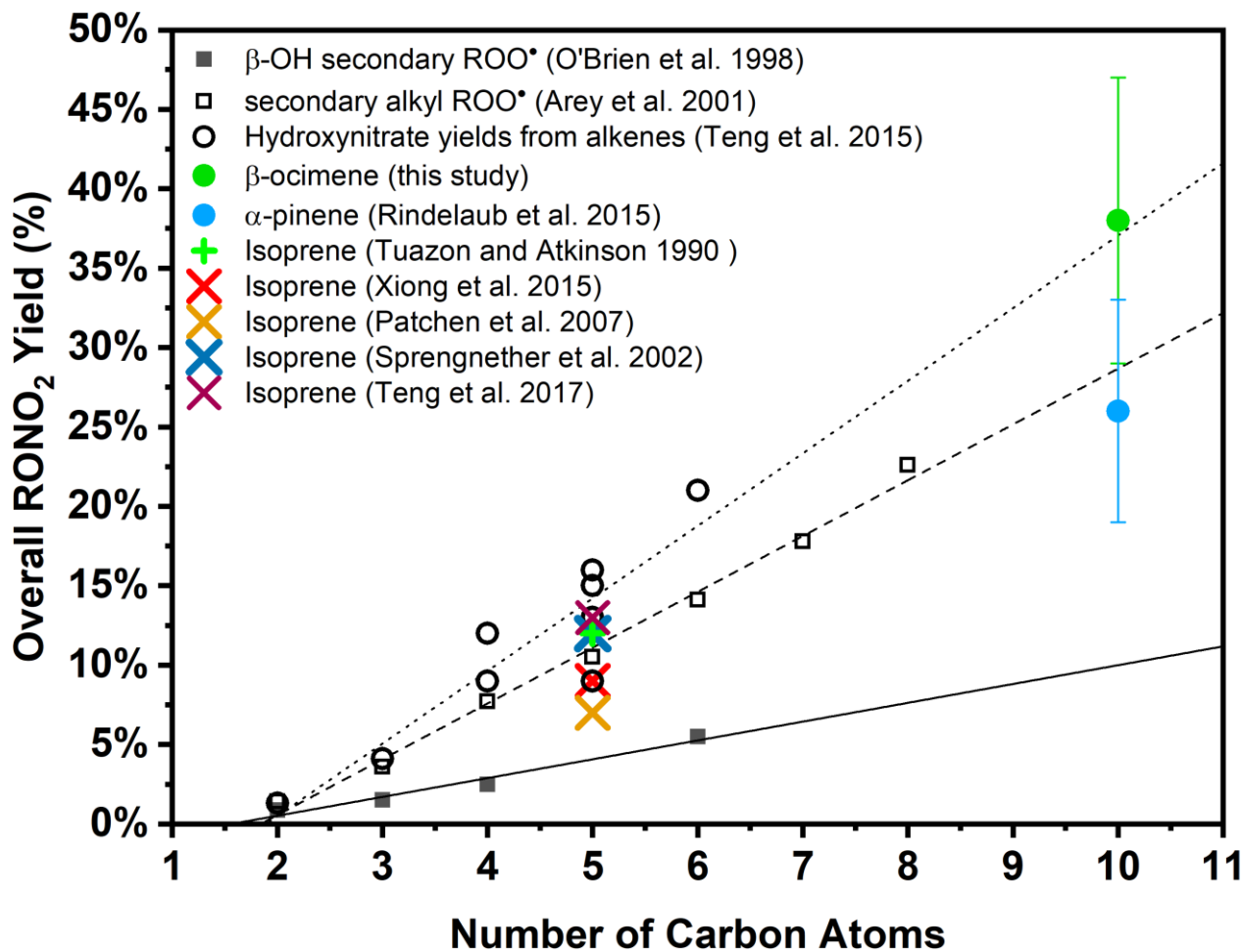
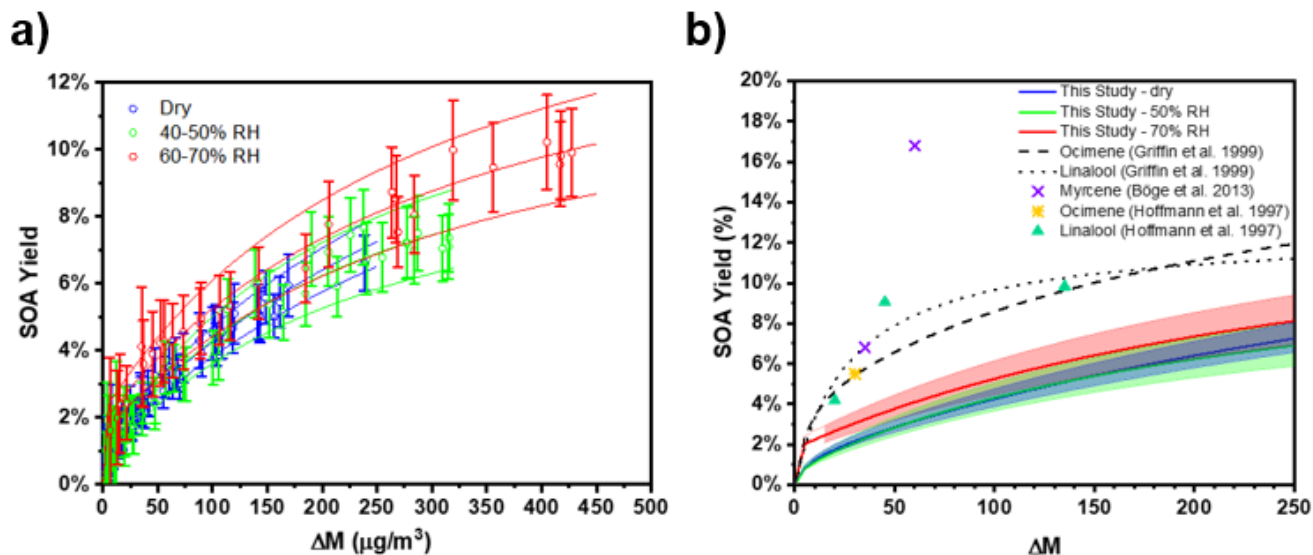


Figure 4: RONO<sub>2</sub> yield vs size for alkyl peroxy radicals. Trend lines are representative for the data sets investigated in O'Brien et al. (1998) ( $\beta$ -hydroxy nitrates from  $\beta$ -hydroxyperoxy radicals), Arey et al. (2001) (alkyl nitrates from secondary alkyl peroxy radicals, alkanes), and Teng et al. (2015) (absolute hydroxy nitrate yields from alkenes).

825



830 Figure 5: a) Change in PM mass concentration ( $\Delta M$ ) and secondary organic aerosol yields for seeded  
 experiments under different RH conditions. The solid lines indicate the two-product absorptive partitioning  
 model fit and the dashed lines represent the 95% confidence intervals of the fitting function. b) Two-product  
 absorptive partitioning model fits of this study vs model fits and SOA yield % reported in the literature for  
 835 the acyclic triolefinic and oxygenated terpenes. The shaded regions represent the 95% confidence intervals  
 of the fitting function. The fitting parameters are as follows:  $\alpha_1 = 0.1768$ ,  $\alpha_2 = 0.0139$ ,  $k_1 = 0.0020$ ,  $k_2 =$   
 0.1698.

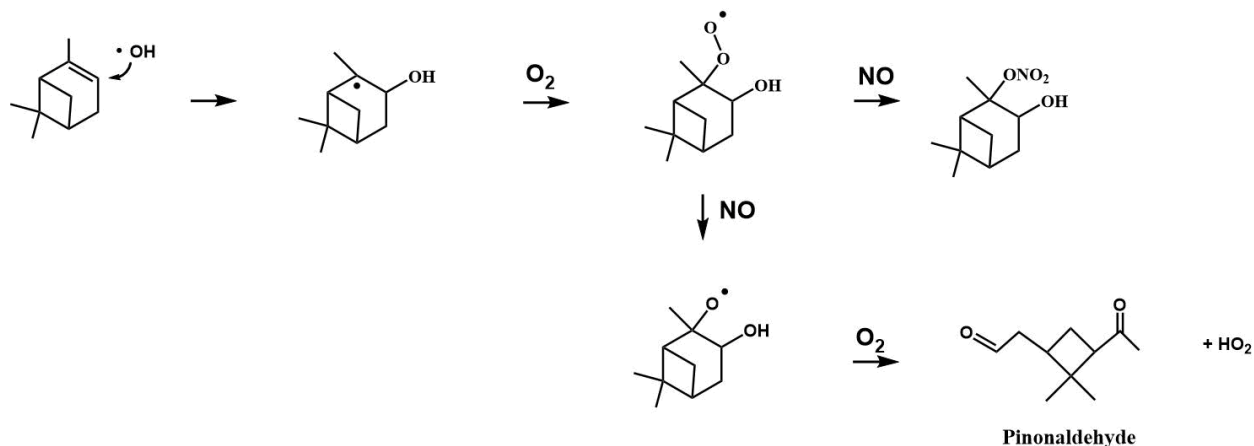
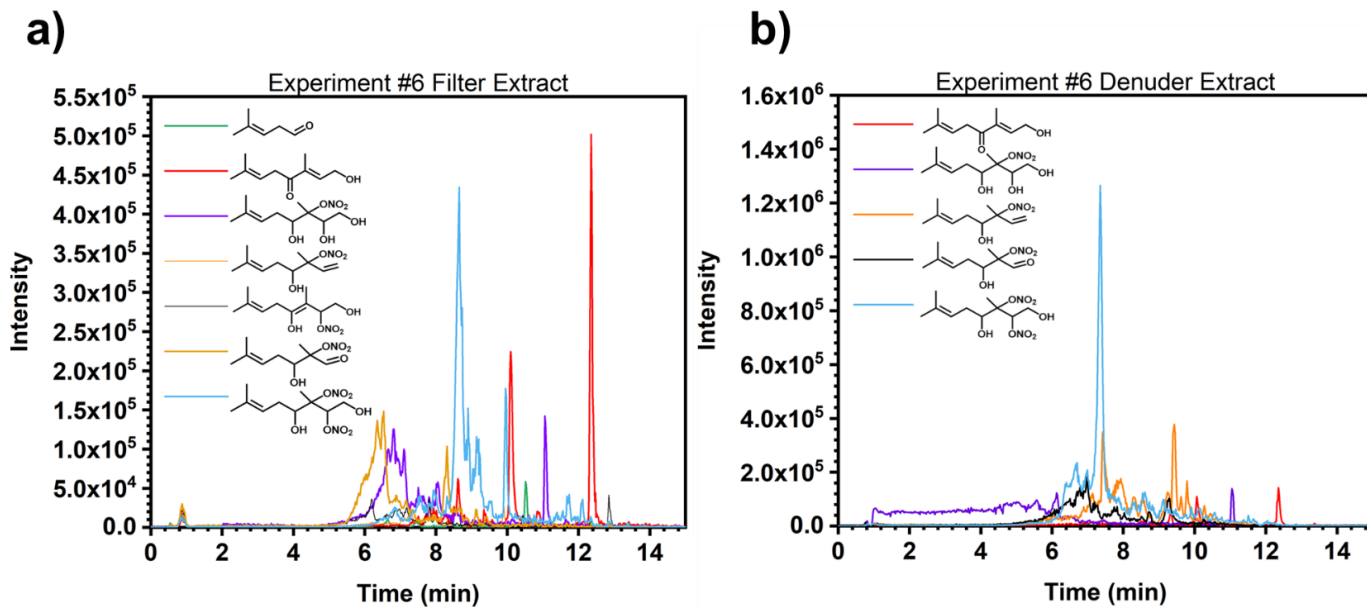
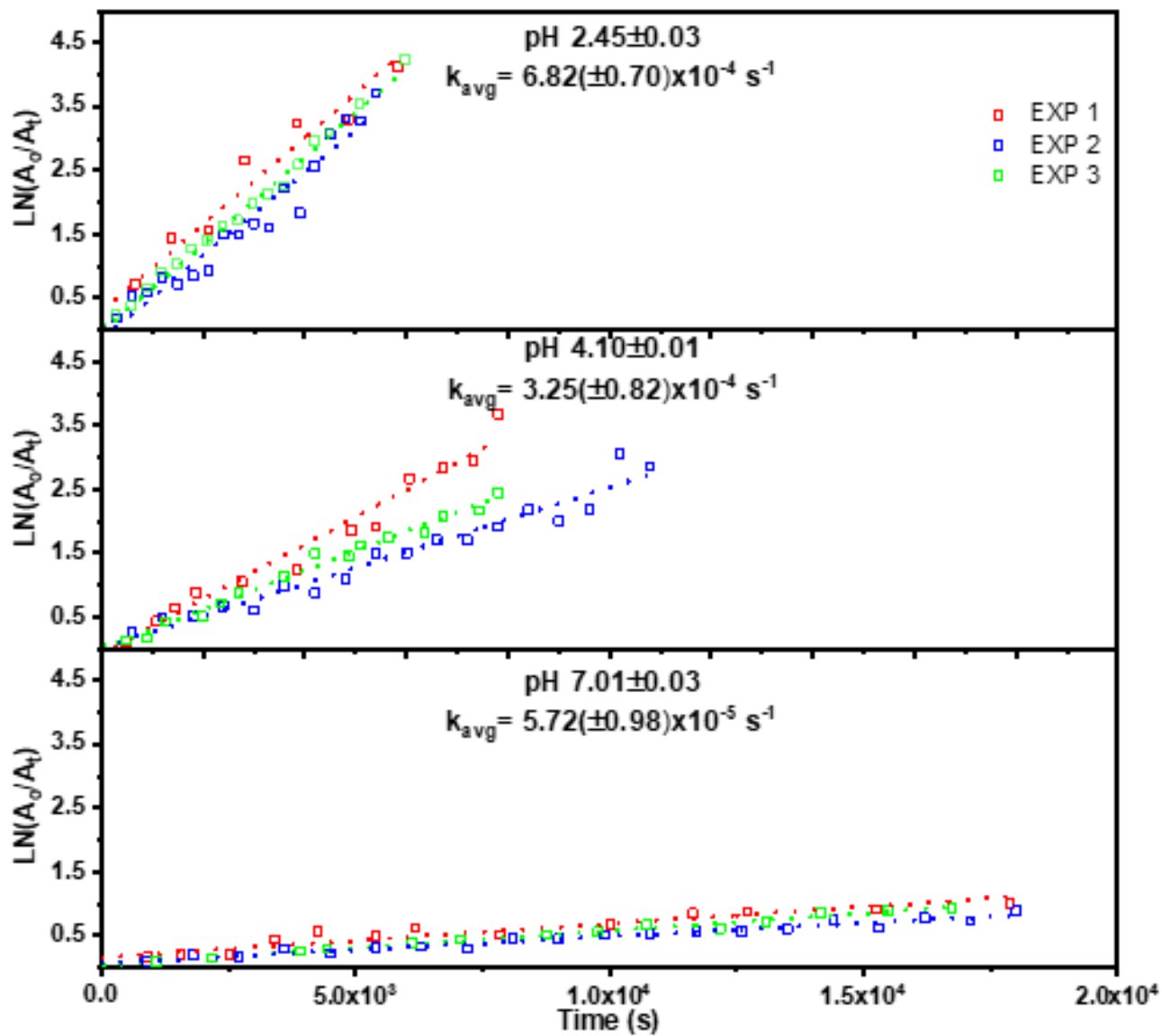


Figure 6: Example reaction pathways of the OH-initiated oxidation of  $\alpha$ -pinene in the presence of  $\text{NO}_x$ .



840

**Figure 7: Selected ion chromatograms (SIC) of expected oxidation products in electrospray (ESI) negative mode for experiment #6 in the a) filter extract and b) denuder extract. Structures listed are tentative assignments of neutral molecules based on the molecular formula of the selected ions. Actual structures may vary depending on the primary addition of the OH.**



845

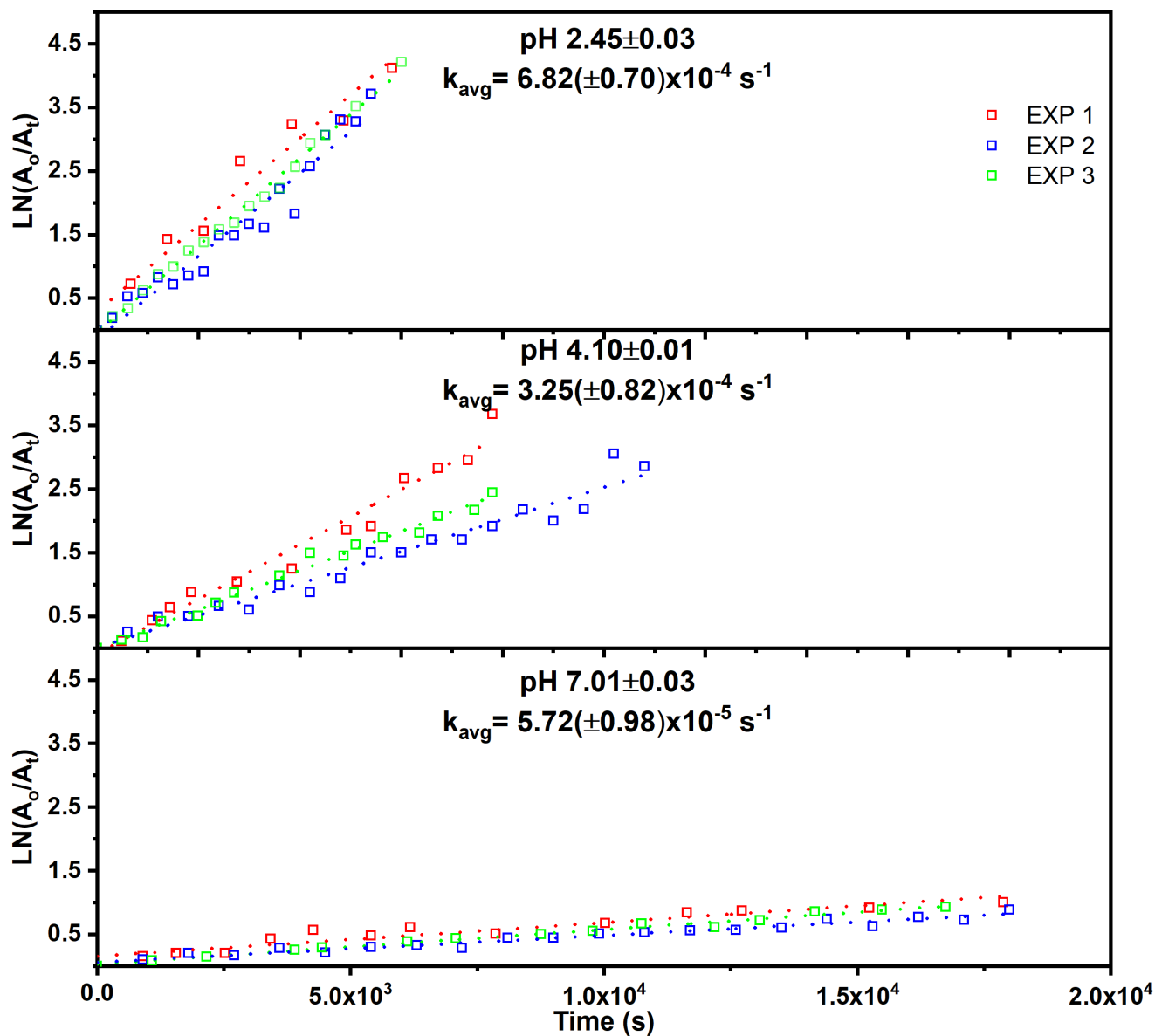
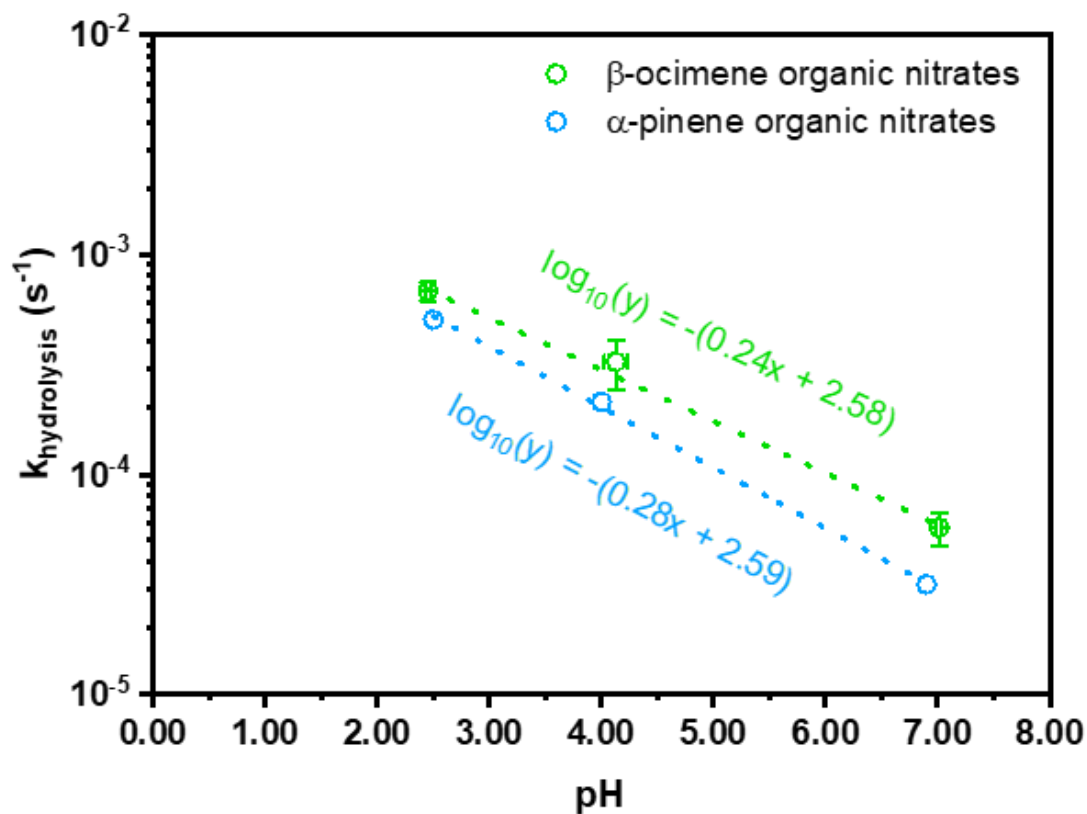


Figure 8: Hydrolysis rate constants for the bulk (gas- and particle-phase) organic nitrates at different pHs. Each pH was analyzed in triplicate and the  $k_{\text{avg}}$  is the average slope of each of the 3 trials.



850 **Figure 9:** Hydrolysis rate constant for  $\beta$ -ocimene hydroxy nitrates (this study, green) and  $\alpha$ -pinene hydroxy nitrates (Rindelaub et al., 2015, blue) as a function of pH. The lines of best fit are listed in the colors corresponding to each monoterpene organic nitrates. Error bars represent the standard deviation between measurements of both the hydrolysis rate constant (y-error) and pH (x-error).

Exp #	Seed	Irradiation time (min)	RH (%)	$\Delta$ [ $\beta$ -Ocimene] (ppb)	$\Delta$ [NO] (ppb)	$\Delta$ [NO <sub>2</sub> ] (ppb)	$\Delta$ [SOA mass] ( $\mu\text{g m}^{-3}$ )	Gas phase - ONO <sub>2</sub> Yield (%)	Particle phase - ONO <sub>2</sub> Yield (%)	Hydroxynitrate Yield (%)
1	(NH <sub>4</sub> ) <sub>2</sub> SO <sub>4</sub>	19	<3%	266 ± 67	509 ± 57	475 ± 45	96 ± 10	nm	nm	nm
2	(NH <sub>4</sub> ) <sub>2</sub> SO <sub>4</sub>	54	<3%	223 ± 30	392 ± 29	284 ± 14	63 ± 5	Nm	nm	nm
3 <sup>a</sup>	(NH <sub>4</sub> ) <sub>2</sub> SO <sub>4</sub>	82	<3%	1357 ± 102	2604 ± 101	nm	933 ± 62	<del>242</del> ± <del>65</del> % <del>4227</del> ± <del>116</del> %	4.1% ± 1.1%	7(+2/-5)%
4	(NH <sub>4</sub> ) <sub>2</sub> SO <sub>4</sub>	73	<3%	425 ± 58	914 ± 13	587 ± 24	nm	% ± % <del>118</del>	1.5% ± 0.5%	6(+2/-4)%
5	(NH <sub>4</sub> ) <sub>2</sub> SO <sub>4</sub>	78	<3%	645 ± 49	1448 ± 11	817 ± 40	nm	<del>358</del> ± % <del>3340</del> ± <del>118</del>	1.6% ± 0.4%	nm
6	(NH <sub>4</sub> ) <sub>2</sub> SO <sub>4</sub>	82	<3%	516 ± 44	1540 ± 11	852 ± 33	143 ± 11	% ± % <del>107</del>	1.3% ± 0.3%	7(+2/-5)%
7	(NH <sub>4</sub> ) <sub>2</sub> SO <sub>4</sub>	102	<3%	524 ± 48	1091 ± 19	856 ± 33	189 ± 14	<del>371</del> ± %	1.3% ± 0.3%	9(+2/-6)%
8	none	95	<3%	653 ± 45	1691 ± 11	1021 ± 38	101 ± 6	<del>296</del> ± <del>86</del> % <del>2049</del>	1.5% ± 0.4%	8(+2/-5)%
9	(NH <sub>4</sub> ) <sub>2</sub> SO <sub>4</sub>	92	46%	556 ± 44	1545 ± 52	1041 ± 38	238 ± 17	% ± <del>44</del> % <del>2048</del>	1.2% ± 0.3%	nm
10	(NH <sub>4</sub> ) <sub>2</sub> SO <sub>4</sub>	89	49%	692 ± 47	2019 ± 11	1185 ± 43	277 ± 24	% ± <del>43</del> % <del>1843</del>	0.9% ± 0.2%	7(+2/-5)%
11	none	19	<3 - 54% <sup>b</sup>	666 ± 38	nm	nm	BDL	% ± <del>43</del> % <del>2248</del>	BDL	6(+2/-4)%
12	(NH <sub>4</sub> ) <sub>2</sub> SO <sub>4</sub>	72	51%	798 ± 48	1913 ± 16	1034 ± 39	315 ± 23	% ± <del>54</del> % <del>1947</del>	1.0% ± 0.2%	3(+2/-2)%
13	(NH <sub>4</sub> ) <sub>2</sub> SO <sub>4</sub>	84	70%	641 ± 46	1628 ± 12	721 ± 41	269 ± 19	% ± <del>43</del> % <del>1745</del>	0.2% ± 0.2%	2(+1/-1.3)%
14	none	24	67%	407 ± 56	474 ± 11	90 ± 30	BDL	% ± <del>43</del> % <del>1443</del>	0.8% ± 0.2%	nm
15	(NH <sub>4</sub> ) <sub>2</sub> SO <sub>4</sub>	92	69%	783 ± 47	1643 ± 10	1209 ± 51	417 ± 26	% ± <del>33</del> %	0.8% ± 0.2%	nm
16	(NH <sub>4</sub> ) <sub>2</sub> SO <sub>4</sub>	86	13%	648 ± 49	nm	nm	238 ± 18	<del>265</del> ± 6%	1.7% ± 0.5%	nm
17	(NH <sub>4</sub> ) <sub>2</sub> SO <sub>4</sub>	87	<3%	569 ± 41	1418 ± 20	878 ± 39	231 ± 18	<del>342</del> ± <del>78</del> %	1.8% ± 0.5%	nm
18	(NH <sub>4</sub> ) <sub>2</sub> SO <sub>4</sub>	88	<3%	560 ± 47	1256 ± 16	666 ± 27	156 ± 12	<del>354</del> ± 8%	1.6% ± 0.4%	nm

a-high concentration experiment. Did not used for yield calculations; b-Irradiated under dry conditions, then increased RH in dark up to 54%

nm-not measured; BDL-below the detection limit



855 **Table 1: Experimental conditions and yield summary of individual experiments. Error represents the propagated analytical uncertainty.**

**Table 2: Buffer systems used for hydrolysis studies and their corresponding pHs.**

Experimental pH	Buffer	pKa
$7.01 \pm 0.03$	$\text{H}_2\text{PO}_4^-/\text{HPO}_4^{2-}$	7.2
$4.10 \pm 0.01$	$\text{CH}_3\text{COOH}/\text{CH}_3\text{COO}^-$	4.8
$2.45 \pm 0.03$	$\text{HSO}_4^-/\text{SO}_4^{2-}$	2.0

860 **Table 3: Hydrolysis rate constants and lifetimes reported in literature.**

Species	Hydrolysis Rate (s <sup>-1</sup> )	$\tau_{\text{hydrolysis}}$ (hr)	Type of Study	Study
all tertiary and non-tertiary RONO <sub>2</sub> <sup>a</sup>	$2.78 \times 10^{-4} \text{ s}^{-1}$	1	Field study + model	Fisher et al., 2016
tertiary RONO <sub>2</sub> from trimethyl benzene <sup>a</sup>	$4.63 \times 10^{-5} \text{ s}^{-1}$	6	Chamber	Liu et al., 2012
methyl nitrate*	$2.14 \times 10^{-8} \text{ s}^{-1}$	13000	Bulk	Baker and Easty, 1952
ethyl nitrate*	$1.07 \times 10^{-8} \text{ s}^{-1}$	26000		
ethyl nitrate <sup>b</sup>	$1.11 \times 10^{-4} \text{ s}^{-1}$	2.5	Bulk	Hu et al., 2011
isopropyl nitrate*	$5.24 \times 10^{-8} \text{ s}^{-1}$	5300	Bulk	Baker and Easty, 1952
isopropyl nitrate <sup>b</sup>	$1.26 \times 10^{-4} \text{ s}^{-1}$	2.2	Bulk	Hu et al., 2011
isopropyl nitrate, pH 0.25	$9.92 \times 10^{-6} \text{ s}^{-1}$	28	Bulk	Rindelaub et al., 2016
isopropyl nitrate, pH 1.7	$3.31 \times 10^{-7} \text{ s}^{-1}$	840		
isopropyl nitrate, pH 4.0	$3.86 \times 10^{-7} \text{ s}^{-1}$	720		
isopropyl nitrate, pH 6.9	$< 4.82 \times 10^{-8} \text{ s}^{-1}$	$> 5760$		
tert-butyl nitrate*	$3.19 \times 10^{-3} \text{ s}^{-1}$	0.087	Bulk	Baker and Easty, 1952
isobutyl nitrate, pH 0.25	$1.12 \times 10^{-5} \text{ s}^{-1}$	23	Bulk	Rindelaub et al., 2016
isobutyl nitrate, pH 1.7	$3.51 \times 10^{-7} \text{ s}^{-1}$	792		
isobutyl nitrate, pH 4.0	$4.13 \times 10^{-7} \text{ s}^{-1}$	672		
isobutyl nitrate, pH 6.9	$< 4.82 \times 10^{-8} \text{ s}^{-1}$	$> 5760$		
1-nitrato-2,3-butanediol	$< 1.11 \times 10^{-7} \text{ s}^{-1}$	$> 2500$	Bulk	Darer et al., 2011
1-nitrooxy-2-hydroxy butane <sup>b</sup>	$1.63 \times 10^{-4} \text{ s}^{-1}$	1.7	Bulk	Hu et al., 2011
2-nitrooxy-1-hydroxy butane <sup>b</sup>	$1.46 \times 10^{-4} \text{ s}^{-1}$	1.9		
2-nitrooxy-3-hydroxy butane <sup>b</sup>	$1.85 \times 10^{-4} \text{ s}^{-1}$	1.5		
2-nitrooxy-2-methyl-3-hydroxy propane <sup>b</sup>	$9.26 \times 10^{-3} \text{ s}^{-1}$	0.03		
3-nitrooxy-2-hydroxy-3-methyl butane <sup>b</sup>	$9.92 \times 10^{-3} \text{ s}^{-1}$	0.028		
2-nitrooxy-3-hydroxy-2,3-methyl butane <sup>b</sup>	$1.46 \times 10^{-2} \text{ s}^{-1}$	0.019		
tertiary isoprene ON*	$9.26 \times 10^{-5} \text{ s}^{-1}$	3	Field study + model	Zare et al., 2018
1-hydroxy-4-nitrooxy isoprene*	$6.76(\pm 0.09) \times 10^{-3} \text{ s}^{-1}$	0.04	Bulk	Jacobs et al., 2014
4-hydroxy-3-nitrooxy isoprene*	$1.59(\pm 0.03) \times 10^{-5} \text{ s}^{-1}$	17.5		
1-hydroxy-2-nitrooxy-3-butene*	$9.95(\pm 0.30) \times 10^{-6} \text{ s}^{-1}$	27.9		
2-methyl-2-nitrato-1,3,4-butanetriol*	$4.15 \times 10^{-4} \text{ s}^{-1}$	0.67	Bulk	Darer et al., 2011
3-methyl-1-nitrato-2,3,4-butanetriol*	$< 1.11 \times 10^{-7} \text{ s}^{-1}$	$> 2500$		
2-methyl-2-nitrato-1,4-butanediol*	$4.55 \times 10^{-3} \text{ s}^{-1}$	0.061		
3-methyl-3-nitrato-1,2-butanediol*	$2.31 \times 10^{-3} \text{ s}^{-1}$	0.12		
$\beta$ -pinene ON (from NO <sub>3</sub> ) <sup>a</sup>	$(6.17\text{-}9.26) \times 10^{-5} \text{ s}^{-1}$	3-4.5	Chamber	Boyd et al., 2015
tertiary $\beta$ -pinene ON*	$9.26 \times 10^{-5} \text{ s}^{-1}$	3	Field study + model	Pye et al., 2015

$\alpha$ -pinene ON <sup>a</sup>	$2.31 \times 10^{-5} \text{ s}^{-1}$	12	Chamber	Bean and Hildebrandt Ruiz, 2016
$\alpha$ -/ $\beta$ -pinene ON, pH 4.60	$> 5.56 \times 10^{-4} \text{ s}^{-1}$	$< 0.5$	Chamber	Takeuchi and Ng, 2019
$\alpha$ -pinene hydroxynitrate, pH 0.25	$1.98 \times 10^{-3} \text{ s}^{-1}$	0.14	Bulk	Rindelaub et al., 2016
$\alpha$ -pinene hydroxynitrate, pH 1.0	$3.81 \times 10^{-6} \text{ s}^{-1}$	0.73		
$\alpha$ -pinene hydroxynitrate, pH 6.90	$3.16 \times 10^{-5} \text{ s}^{-1}$	8.80	Bulk	Rindelaub et al., 2015
$\alpha$ -pinene hydroxynitrate, pH 4.00	$2.14 \times 10^{-4} \text{ s}^{-1}$	1.30		
$\alpha$ -pinene hydroxynitrate, pH 2.50	$5.05 \times 10^{-4} \text{ s}^{-1}$	0.55		
$\beta$ -ocimene hydroxynitrate, pH 7.01( $\pm$ 0.03)	$5.72(\pm 0.41) \times 10^{-5} \text{ s}^{-1}$	$4.9 \pm 0.8$	Bulk	This study
$\beta$ -ocimene hydroxynitrate, pH 4.13( $\pm$ 0.01)	$3.25(\pm 0.12) \times 10^{-4} \text{ s}^{-1}$	$0.85 \pm 0.22$	Bulk	
$\beta$ -ocimene hydroxynitrate, pH 2.45( $\pm$ 0.03)	$6.82(\pm 0.36) \times 10^{-4} \text{ s}^{-1}$	$0.4 \pm 0.05$	Bulk	

a- pH of the solution was not given.

b- For primary and secondary systems, the acid-catalyzed mechanism hydrolysis lifetime (for 55 wt % D2SO4 solution) is given.

\*-Neutral hydrolysis lifetime is given.